AAEC/PR41-P
INDC(AUL)-23/G

NOT FOR PUBLICATION
See note overleaf

XA04N2775

AAEC/PR41-P
INDC(AUL)-23/G

INIS-XA-N--163

AUSTRALIAN ATOMIC ENERGY COMMISSION

RESEARCH ESTABLISHMENT

LUCAS HEIGHTS

PROGRESS REPORT OF PHYSICS DIVISION

1st AUGUST, 1974-30th SEPTEMBER, 1975

ACTING DIVISION CHIEF - MR. W. GEMMELL

NOT FOR PUBLICATION

This report was printed for circulation within the Australian Atomic Energy Commission. It has not been reviewed for general issue.

It is made available on the understanding that the information it contains will not be quoted in publications, listed in abstract journals or communicated to the Press.

AUSTRALIAN ATOMIC ENERGY COMMISSION

RESEARCH ESTABLISHMENT

LUCAS HEIGHTS

PROGRESS REPORT OF PHYSICS DIVISION

1st JULY, 1974 - 30th JUNE, 1975

ACTING DIVISION CHIEF - MR. W. GEMMELL

CONTENTS

CONTENTS (cont'd)

CONTENTS (cont'd)

CONTENTS (cont'd)

1.1 INTRODUCTION

Customer satisfaction with the introduced uranium analysis service has produced additional requests for service type assistance. Two are currently being studied: a quick method of analysis for thorium and characterisation of the source of obsidian archaeological artefacts. Several nuclear techniques have been brought to bear on obsidian with consistent and reproducible results. Source material has been identified of unknown origin. The techniques are now being used to study trading patterns by the movement of obsidian flakes between the Pacific Islands.

The neutron capture cross sections for more isotopes have been analysed. The data in the 3 to 300 keV energy range was obtained at the Oak Ridge Electron Linear Accelerator facility in 1972. In addition to providing accurate neutron capture cross sections and resonance parameters suitable for inclusion in neutron data libraries, the information yielded provided a good test of several of the current theories of nuclear structure - valence model and doorway states.

Several reviews of problem areas in nuclear energy were undertaken. Of particular note are those on 'Hydraulic Methods for Blowdown of Water Cooled Reactors', 'The Storage and Disposal of Radioactive Waste' and 'The Technological Problems of Fusion Reactors'.

An examination of our knowledge of oceanic transport of pollutants has followed on from the examination of the radioactive waste disposal options.

In addition to the development of a code - NAIAD - for the analysis of blowdown, analytical work on the well documented SPERT experiments has produced a satisfactory quantitative explanation without invoking ad hoc assumptions. The method is now being applied to safety studies of the two local reactors.

The proposals for experimental study of water flow on the White's mining tailings mound at Rum Jungle received a setback as a result of cyclone Tracy. Preparations are now complete to install a weir on the White's mound during the dry season. This will provide a record of water flow and, together with records of rainfall and ion concentrations in the run-off water, should provide a sound basis for further analysis and modelling. A code, capable of predicting air and water flow within the mound for discontinuous rainfall patterns, is at an advanced stage of development. It is currently being checked out against laboratory experiments.

Our operational efficiency of the IBM 360 computer has been markedly improved by the introduction of a PDP-11/10 processor which acts as a remote job input/output terminal. This small local computer also provides interactive text and graphic facilities. Significant development work is envisaged to make full use of its potentialities, e.g. previewing data stored on the IBM 360 prior to hard copy being drawn by a Calcomp plotter.

2.1 MOATA REACTOR OPERATIONS (T. Wall)

Significant use of the reactor during the period was made by the following projects.

Uranium Ore Analysis	Student Training
Neutron Activation Analysis	Minor Isotopes Production
Prompt Nuclear Analysis	Reactor Transient Studies
Neutron Radiography	

Forty-four megawatt hours of operation were logged between July 1, 1974 and June 30, 1975, bringing the total burn-up to 100 MWh since routine 100 kW operation commenced. Two new fuel plates were added to the core in place of aluminium dummies to restore reactivity lost through burn-up. Projected increases in service demands will, if realised, increase the rate of burn-up to about 100 MWh per year. On current estimates, a changeover from 12 to 13 plate fuel elements will then be necessary by the end of 1976.

Uranium Ore Analysis

This commercially available service has been well received and more than 2500 samples have been analysed. Upgrading of the data collection and recording equipment for the rig is in hand to meet the projected requirements of the Uranium Exploration Division. Consideration is also being given to the provision of a stand-by rig on HIFAR.

Neutron Radiography

Neutron radiography offers greater contrast to conventional X-ray radiography as a NDT technique and has found extensive use in the examination of objects with components made from mixtures of metallic, hydrogenous and non-metallic materials.

The facilities on the reactor MOATA have been developed to provide a neutron radiography service. During the year ending July 31, 1975, 50 emergency door thrusters from Boeing 747 aircraft have been neutron radiographed on a service basis for Qantas Airways Ltd. The use of neutron radiography enabled the presence and correct location of 'O' ring seals, explosive charge and transmission oil to be confirmed for the assembled component (Figures 2.1 and 2.2). Insufficient contrast would have been obtainable by X-ray methods for definitive results.

About 100 small explosive detonators have been examined in service work for the Munitions Filling Factory, St. Mary's, N.S.W. During this investiga-

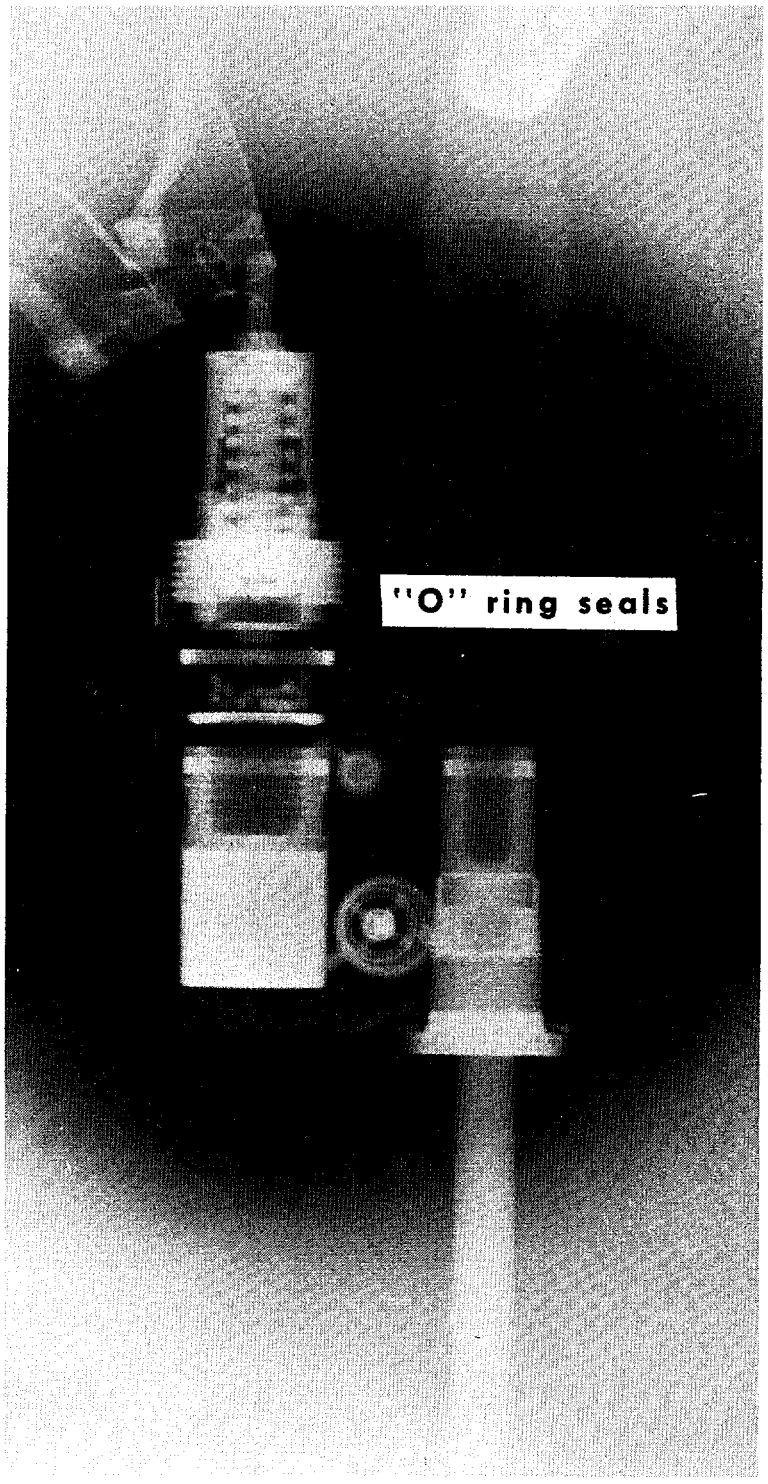

Figure 2.1 Neutron radiograph of Boeing 747 emergency door thruster

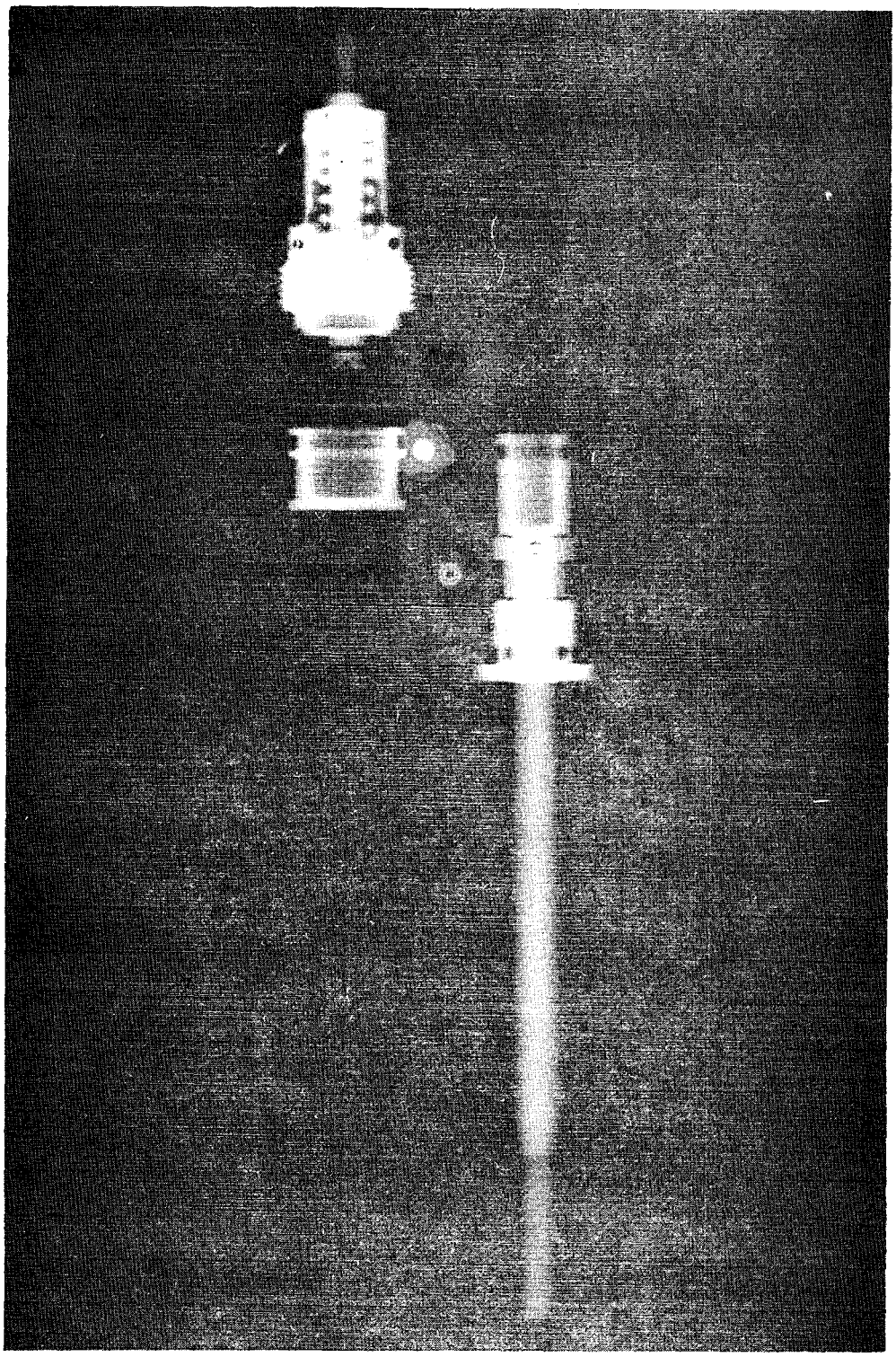

Figure 2.2 X-ray radiograph of Boeing 747 emergency door thruster

Figure 2.3 Neutron radiograph of explosive detonator

tion several faulty detonators were detected (Figure 2.3). As a result, a modification was made to the manufacturing specification for this detonator. Subsequent re-examination of detonators after the modification revealed that the process was successful. Again, X-ray methods would have given insufficient contrast for definitive conclusions to be made.

Investigation has been made into the use of a low strength ^{252}Cf neutron source in combination with highly sensitive neutron detector/film combinations. Difficulties were experienced with the low neutron source strength (70 μg ^{252}Cf), but some radiographs were obtained using high speed, light sensitive film with a lithium doped glass converter screen. The evaluation of the use of ^{252}Cf in larger source strength still relies on published work from overseas.

Neutron Activation Analysis - Obsidian Volcanic Glass

Obsidian was a rare and valued source material in the manufacture of cutting tools and ornaments by natives of the South West Pacific region. It was extensively traded throughout the region in the last two to three thousand years. The Research School of Pacific Studies, Australian National University, in cooperation with the MOATA services and Nuclear Analysis Groups of Physics Division, are labelling all known sources of obsidian in the region. The six known sources have been studied using three nuclear analysis methods. These are: neutron activation analysis (NAA), proton-gamma analysis (PGA, see sections 3 and 4) and delayed neutron analysis (DNA). Figure 2.4 shows the results of NAA on the source material and a comparison with Figure 3.4 indicates that both NAA and PNA produce similar and strong discrimination be between sources. The use of DNA (Figure 2.5) also provided good discrimination and is currently being used on large sample batches of artefacts because of the decreased costs and analysis time involved.

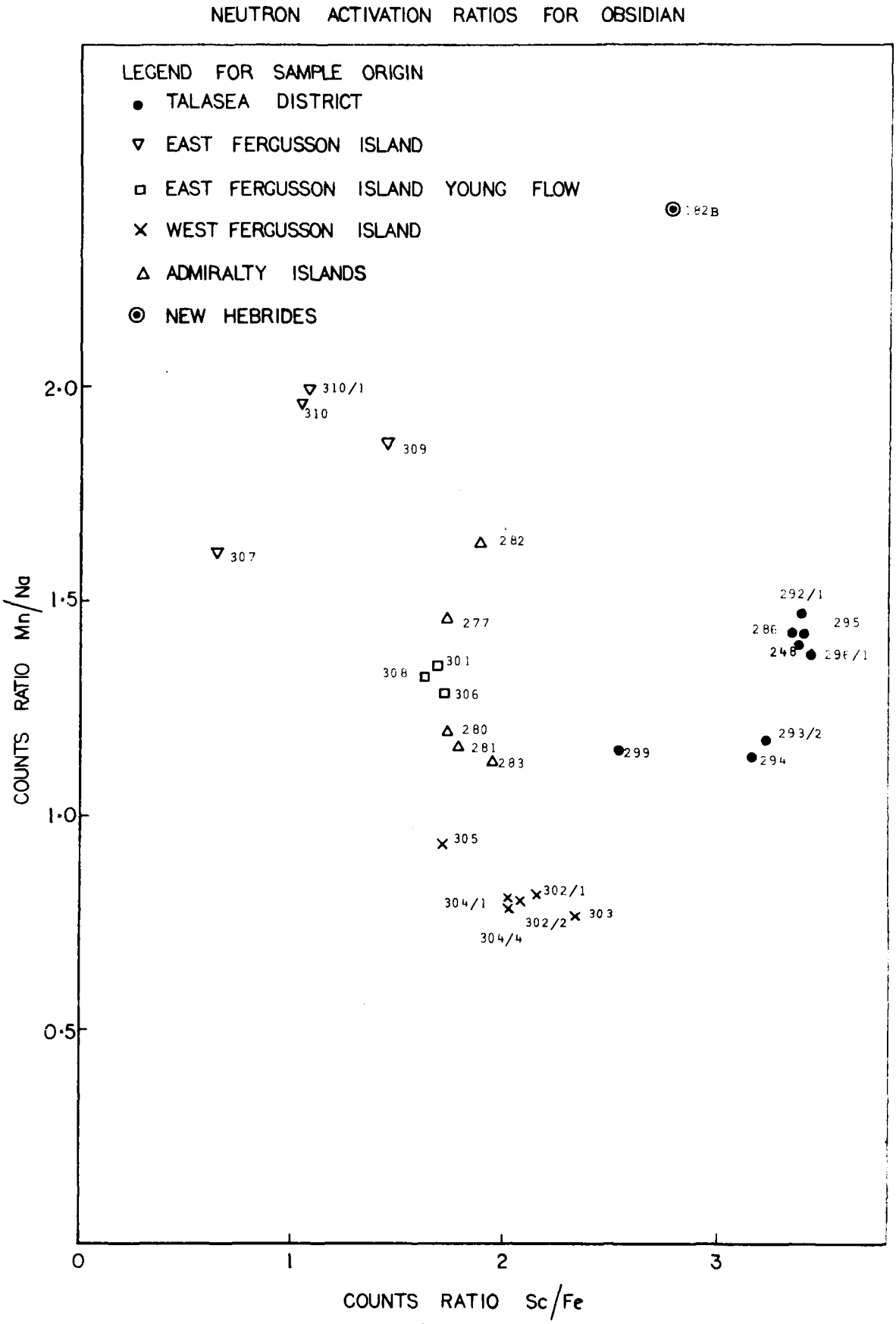

Figure 2.4: Activity ratios of obsidian from various sources

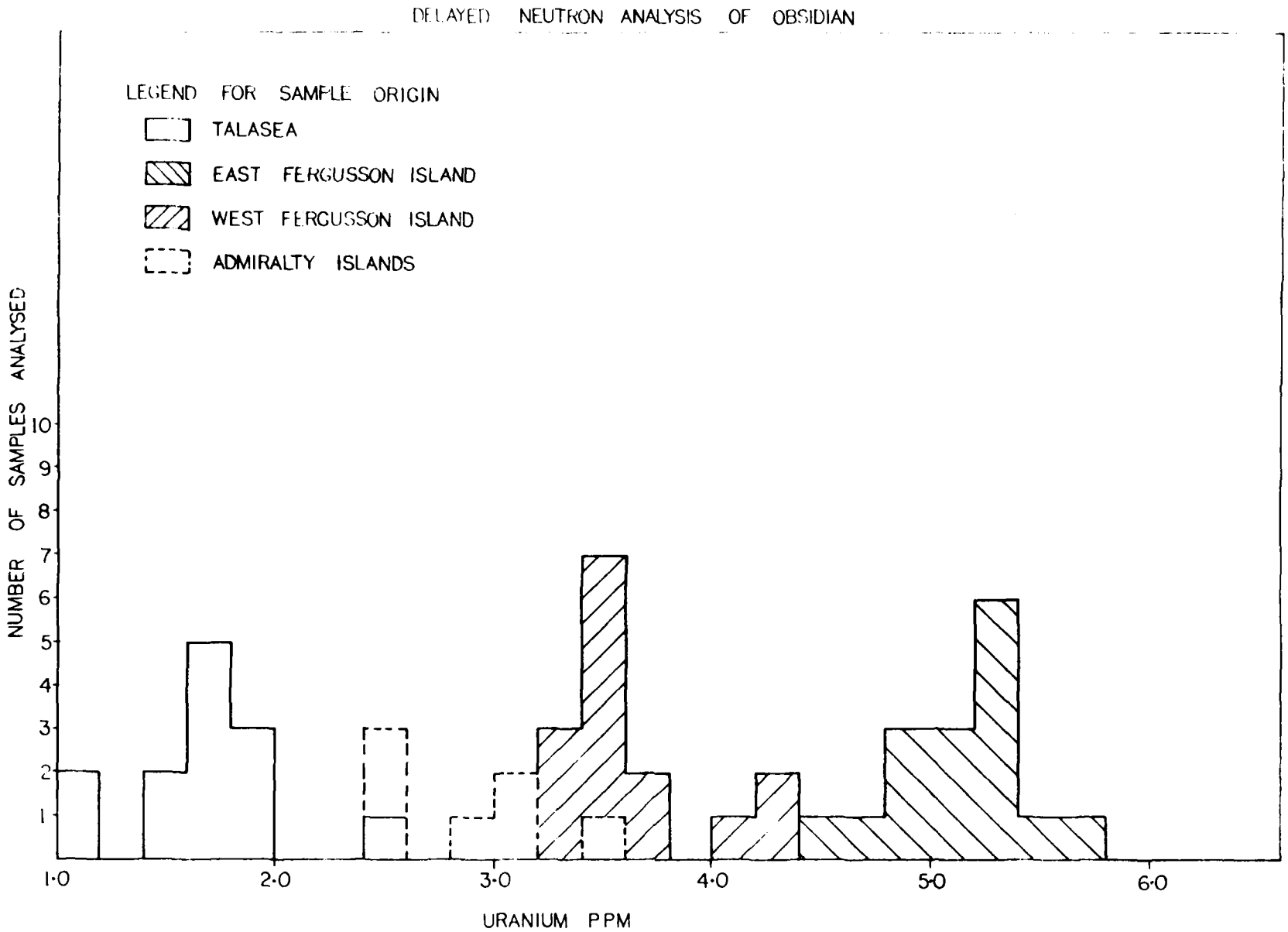

Figure 2.5: Uranium content of obsidian from various sources

2.2 CRITICAL FACILITY (D. B. McCulloch, J. W. Connolly, J. R. Harries, G. Durance, R. B. Knott)

Operation

Construction of the 'hard spectrum' $^{235}U/C$ core, FC1, commenced in October and criticality was achieved early in December. Experimental use of this core has been limited to three days per week, leaving one day per week for a group training and familiarisation program and one day for scheduled maintenance and modification work. It has also enabled analysis to keep reasonable pace with data collection.

Operation of the facility has continued to be satisfactory, with only minor electronic and mechanical malfunctions. Inflatable seals were fitted to the cell door and a pressure test of the cell conducted. After rectification of a leakage path via an incorrectly seated coupler in the experimental cable penetration plate, a leakage rate within specification was obtained.

Experiments

(a) MOATA Mock-up Experiments

Neutron'noise' data obtained from the MOATA mock-up cores have been analysed for both auto- and cross-correlations to determine the prompt neutron decay constants and the coupling parameters between the two cores. The assemblies studied had graphite coupling thicknesses of 450, 600 and 800 mm. Two and three dimensional neutron diffusion codes have been used in the analysis and have highlighted the extreme sensitivity of calculated prompt decay constants to the neutron balance between core tanks and the coupling region.

Cross correlations of the neutron noise in the two slab cores of each assembly have enabled measurement of coupling reactivity, and the time taken for neutrons to travel from one slab to the other. The maximum such time delay was obtained for the 800 mm separation assembly (1.50±0.07 ms).

These assemblies have enabled a study of coupling mechanisms over a range of slab separations without the necessity to consider the influence of core design differences usually encountered when comparing measurements made in different reactors.

(b) Assembly FC1

Loading of fuel to the graphite matrix of the hard spectrum core FC1 (described in the previous Progress Report, AAEC/PR40-P) commenced in December.

Criticality was obtained on December 11 at a fuel loading of 13.14 kg, in excellent agreement with the calculated value of 13.0 kg.

The experimental program for this assembly is primarily intended to explore the problems of making reactor physics measurements in the facility and include:

(i) Neutron noise measurements.

(ii) Proton recoil neutron spectrometry.

(iii) Reaction rate distribution measurements using fission counters and activation detectors.

(iv) Central reactivity worth measurements.

In connection with (iv) considerable effort has been devoted to establishing the limitations to accuracy of reactivity perturbation measurements arising from reproducibility of the 'tables closed' position, control rod critical settings and other unavoidable sources of small reactivity changes. It appears that a precision of the order $\pm 10^{-6}$ $\Delta k/k$ or better is attainable.

(c) Next Assembly

Preliminary appraisal has begun of a ^{235}U fuelled, hydrogenous (polyethylene or polystyrene) moderator configuration of short neutron lifetime for construction early in 1976. A matrix-type assembly using square-section aluminium tubes is envisaged. A primary aim will be measurements of temperature coefficients pertinent to the SPERT transient analyses (section 4.1), both for a water reflector and for localised regions of the core. Neutron noise analysis techniques will be further investigated, probably with extension to a coupled core short lifetime configuration, and it is expected that the assembly may also be suitable for investigation of some neutron streaming effects.

2.3 PULSED INTEGRAL MEASUREMENTS IN HEAVY METAL ASSEMBLIES

Sensitivity Studies (M. Rainbow, I. Ritchie, A. Rose, S. Whittlestone)

Calculations have been extended to cover both the range of source energy conditions which can be attained experimentally and to include ^{238}U assemblies as well as the thorium assemblies previously studied. The calculations show that the time dependent decay rate, the parameter measured experimentally, is primarily sensitive to the value of absorption cross section in the energy range below about 100 keV when a low energy source is used, and to the value of inelastic cross section at energies about 0.5 to 5 MeV when a high energy source is used. This is relevant to the evaluation of data for fast reactor neutronics calculations. For example, the uncertainty which exists in the value of the inelastic cross section for ^{238}U in the range 0.8 to 5 MeV and in the value of the absorption cross section below 50 keV has considerable impact on the economical operation of fast breeder reactors.

The results also show that this type of experiment should be a useful addition to the integral experiments which have been used to elucidate some of the systematic errors that exist in microscopic cross section data.

Pulsed Integral Measurements in Thorium

Further experiments have been carried out which confirm the marked variation with time of the decay rate measured in a thorium assembly with a low energy source. Some of the results are shown in Figure 2.6 together with a diffusion theory calculation using ENDF/B data. Apart from the fact that the calculated results are too high, which may be a consequence of using a diffusion theory calculation, they also show none of the structure present in the experimental results.

Preliminary experiments using small hydrogenous liquid scintillators developed at Lucas Heights to measure time dependent neutron spectra, have given very encouraging results. Good neutron/gamma discrimination has been achieved. The major background count rate due to gammas comes, not from the scintillator, but from gammas impinging on the photocathode of the photomultiplier. This effect should be reduced when the present perspex light guide from scintillator to photomultiplier is replaced by one made of quartz. The quartz light guide will also give better light transmission from scintillator to photomultiplier and eliminate perturbation of the neutron spectrum caused by the hydrogen content of the perspex.

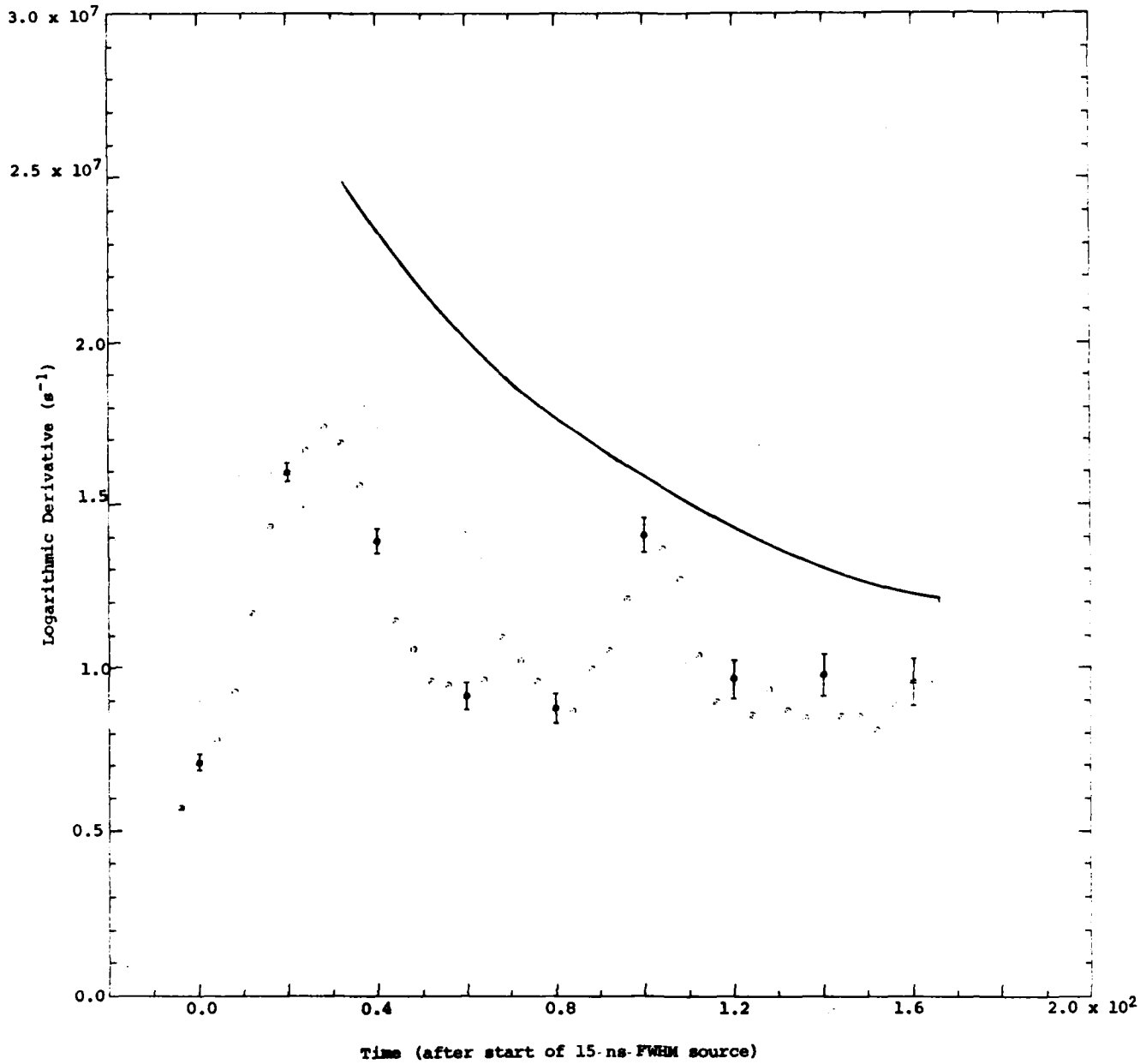

Figure 2.6 Decay constant of ^{235}U reaction rate in a thorium metal assembly: low energy neutrons. Comparison of experiment and theory.

Time-Dependent Spectra in Thorium Stacks

Calculations of the time-dependence of neutron spectra in the thorium stack experiments continued using the ORNL Monte Carlo code MORSE. The actual geometry of the target was included in the calculation with noticeable effect on the calculated results. With such complex geometries, which have to be defined in detail as part of the code data, there is always the possibility of error. As part of the study, the ORNL code PICTURE was made operational. This code takes the input data to MORSE and quickly produces as printed output section drawings of the configuration described by the data. This provides a visual check that the geometry description is correct.

The present series of calculations for the stacks is now complete. In general, these show that the differences noted previously between experiment and simple calculations were not due to the geometrical assumptions made in the calculations. This probably points to deficiencies in the cross section data sets used in calculation.

2.4 SAFETY STUDIES

Loss of Coolant Accident Analysis (W. J. Turner, G. D. Trimble)

A comprehensive critical review was made of hydraulics for blowdown analysis of water cooled reactors (Turner and Trimble 1975)[1]. It concludes that the methods most widely used for the hydraulic analysis of loss of coolant accidents in light water reactors are unsatisfactory and that insufficient use has been made of results and methods in closely related fields. Support for this view is found in the historical review of LOCA analysis. Published blowdown experiments are reviewed and a brief description of the experimental rigs is given. All published comparisons of blowdown experiments and calculations are listed and discussed. It is found that there are almost no grounds for believing that the present LOCA codes can predict the coolant or fuel conditions in a large power reactor during blowdown. However, the extreme conservatism in the US Nuclear Regulatory Commission's licensing rules compensates for this very large margin of ignorance. Still, this large margin is undesirable and the use of inaccurate design tools is very likely to distort design and design objectives with long term safety and economic consequences.

A summary of the NAIAD blowdown code and a comparison of results from it with an Italian blowdown experiment, were presented at the NEA-CPL Seminar on Computer Programs for the Analysis of Certain Problems in Thermal Reactor Safety, held at Ispra, October 1974[2]. The conference paper aroused interest. Since then, NAIAD has been used to calculate the blowdown and reflood of a CANDU test channel and the results compared with those from the AECL code, FIREBIRD. The NAIAD calculation proved to be several times faster than the preliminary FIREBIRD calculation. The final FIREBIRD calculation is still not available so that a detailed comparison has not been made.

Attention has been given to the calculation of two phase flow at or near choked conditions. It has been shown that those two phase flow slip models which give good agreement with density measurements, also give good agreement with pressure gradients for near choked two phase flows (Nahavandi and Von Hollen 1965[3], Turner and Trimble 1974[4], and with choke mass velocity measurements (Trembley and Andrews 1971[5], Turner and Trimble 1974[4]. These results have not been included in LOCA calculations for two reasons. Firstly, in order to simplify the calculation, most LOCA codes (e.g. RELAP-4, Moore and Rettig 1973)[6] assume homogeneous flow which does not give agreement with measured densities, pressure gradients at near choke flows or choked mass velocities. Secondly, there is a large discontinuity in the choke mass velocity calculated

from a slip model at zero quality.

A method has been developed which removes this discontinuity when the choke mass velocity is expressed as a function of stagnation enthalpy and throat pressure. The results for Jones' slip are shown in Figure 2.7. The top two lines are in the superheated steam region, the nearly constant pressure sections are at zero quality, and the remainder is the two phase region. A comparison with the measurements of Fauske (1962)[7] in his TSII test section is shown in Figure 2.8.

Development of the NAIAD blowdown code has continued and many improvements have been incorporated. Among these are:

1. The intrinsic choke flow calculation described above has been incorporated in such a way that any of the available slip models may be used for the choke flow calculation. The last finite difference mesh point is now at the choking throat.

2. The time step size is changed at every time step to take full advantage of the stability of the finite difference scheme.

3. Blowdown of hydraulic networks containing pumps, heat exchangers, etc. can now be done. The most complex problem to date is the blowdown of the primary loop of a CANDU PWR. Both primary and secondary loops were calculated, including pumps in both loops, a reactor core, a heat exchanger and a makeup system. A 40 s blowdown of this system was computed in less than 2 minutes on the AAEC IBM360/50 computer.

---

[1] Turner, W. J. and Trimble, G. D. (1975) - Critical Review - Hydraulics for blowdown analysis of water cooled reactors. NSTB/PE10.

[2] Turner, W. J. and Trimble, G. D. (1974) - NAIAD: A different approach to hydraulic calculations.

[3] Nahavandi, A. N. and Von Hollen, R. F. (1965) - Nucl. Sci. & Eng. 22, 463.

[4] Turner, W. J. and Trimble, G. D. (1974) - 5th Australasian Conf. Hydraulics and Fluid Mechanics, Christchurch, NZ, Dec. 9-13.

[5] Tremblay, P. E. and Andrews, D. G. (1971) - Nucl. Sci. & Eng. 44, 1.

[6] Moore, K. V. and Rettig, W. H. (1973) - RELAP 4 - A computer program for transient thermal-hydraulic analysis. ANCR-1127.

[7] Fauske, H. K. (1962) - ANL-6633.

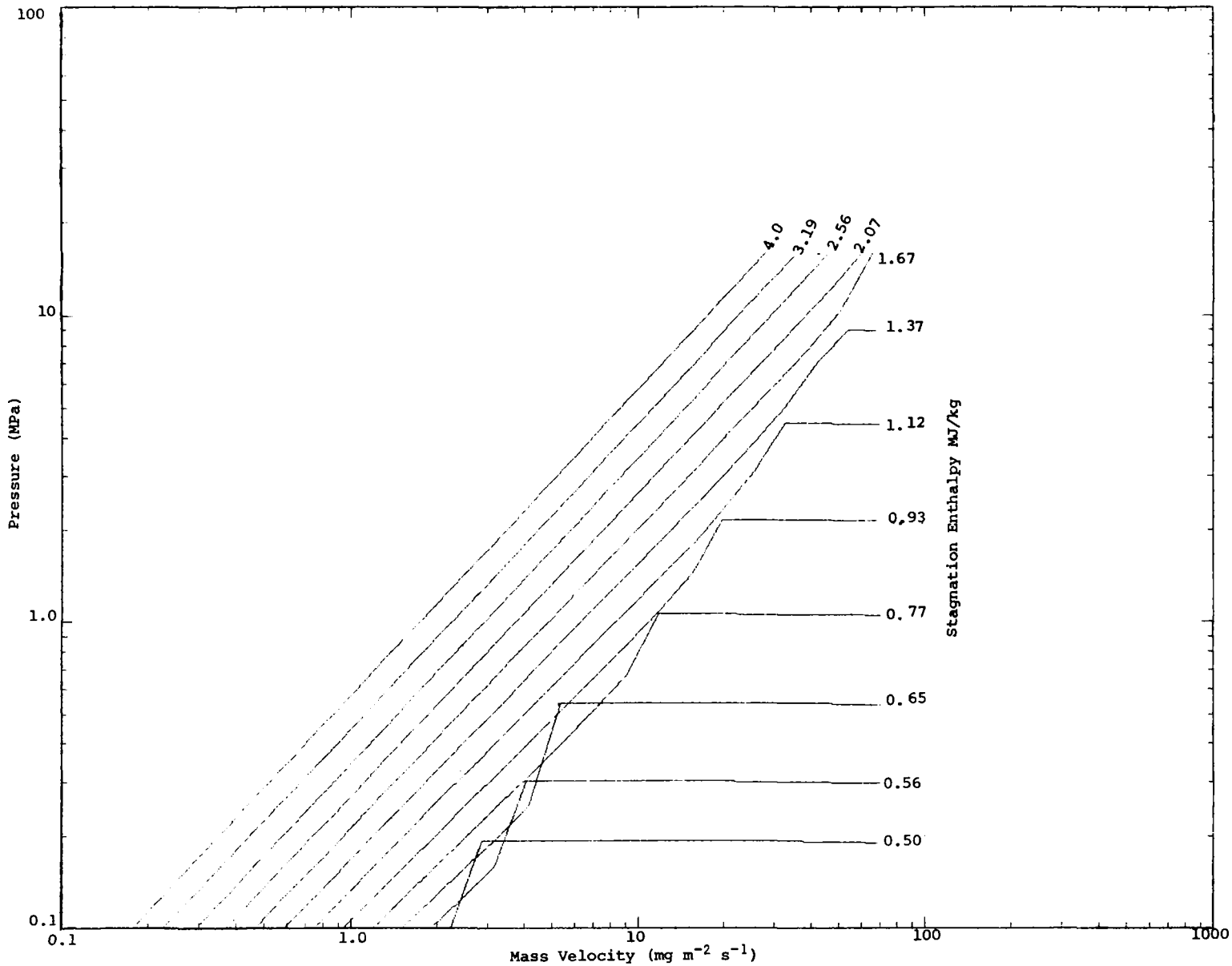

Figure 2.7 Intrinsic choke flow rate for Jones slip

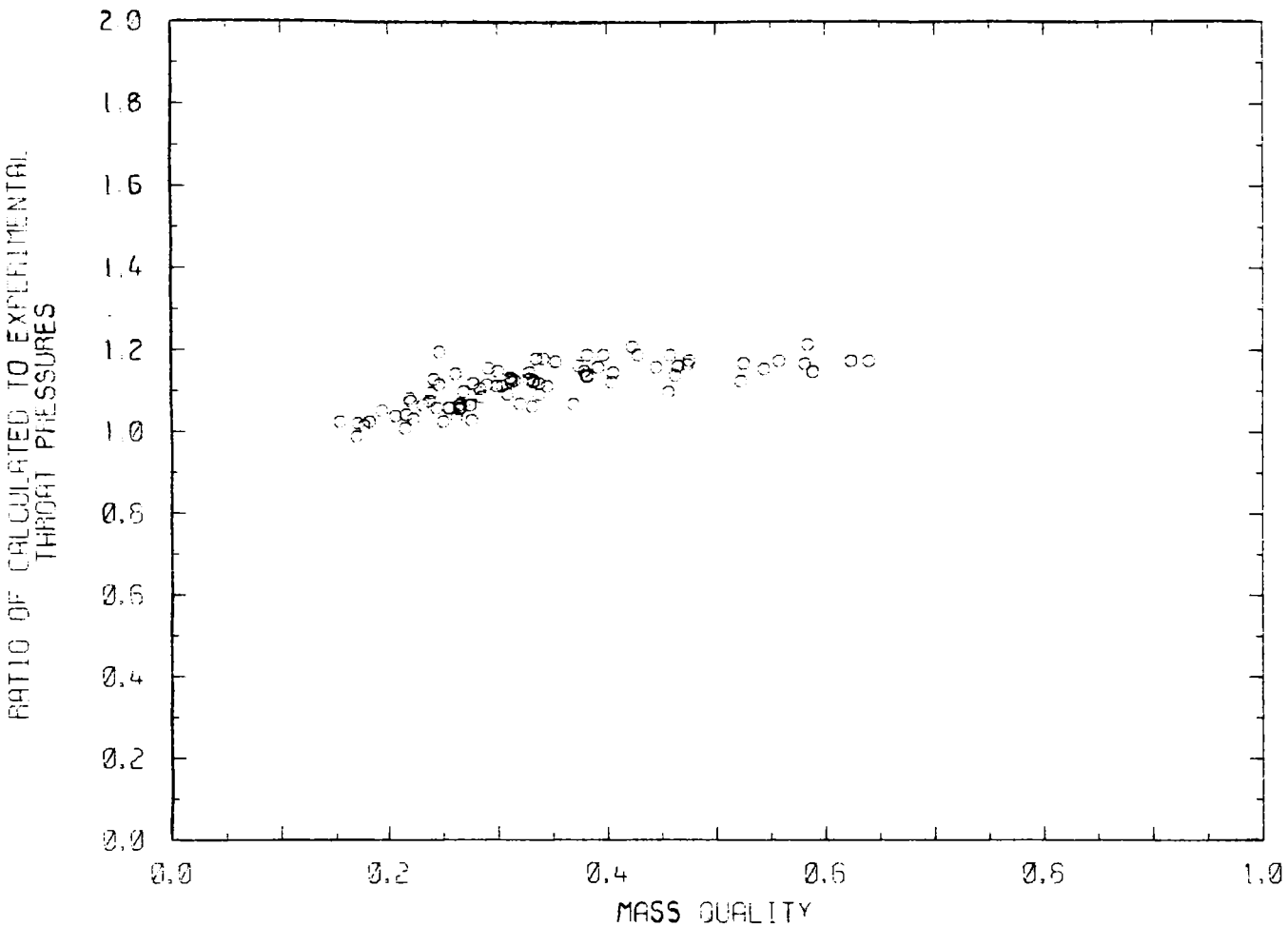

FIGURE 2.8 Throat Pressures for Fauske Test Section II

Analysis of SPERT Power Transients (J. W. Connolly)

Analysis of the effect of increasing the initial temperature of the water moderator in core B29/32 prior to initiating a power transient has shown that for transients terminated by non-boiling processes the variation of burst parameters with initial temperature arises from the temperature dependence of the feedback mechanism. Once boiling shutdown commences, the initial moderator sub-cooling becomes the dominant factor in determining the burst parameters.

The transient power behaviour of the stainless steel fuel plate, boron poisoned reactor P18/19, has been calculated and good agreement obtained with experiment over a range of initial periods of 1 s to 5 ms and maximum fuel plate temperatures up to 500°C.

Reactor physics analysis of the D_2O moderated, close packed core B18/68, proved difficult because of the complicated space and energy dependent neutron leakage. Reasonable agreement with most experimental parameters of this core were finally obtained, except for the overall temperature coefficient. Use of calculated (AUS) core feedback coefficients in ZAPP produced reasonable agreement with experimental power bursts, which was improved by a two region modelling of the reactor core to enable the extremely steep flux gradient at the core reflector interface to be taken into account. The agreement between experimental and calculated energy releases is shown in Figure 2.9.

A model is being developed to allow inclusion of steam voiding and evaluation of the resulting pressure pulse occurring for faster transients after peak power has been passed.

Fuel Coolant Interactions (A. W. Dalton)

The scope of the review of fuel-coolant interaction literature has been much broadened since the previous Progress Report. In addition to the Culham small scale experiment/basic theory approach then described, major attention has been given to the ANL empirical model approach, which they have incorporated into a large scale computer code for reactor safety assessment. Contact has been established with both Culham and ANL groups and is expected to continue.

A critical review of the current status of understanding and analysis of fuel-coolant interactions has been made and the general conclusions drawn can be summarised as follows.

On the basis of the ANL model LMFBR systems appear to be inherently safe with regard to the FCI, especially if film boiling is taken into account, but

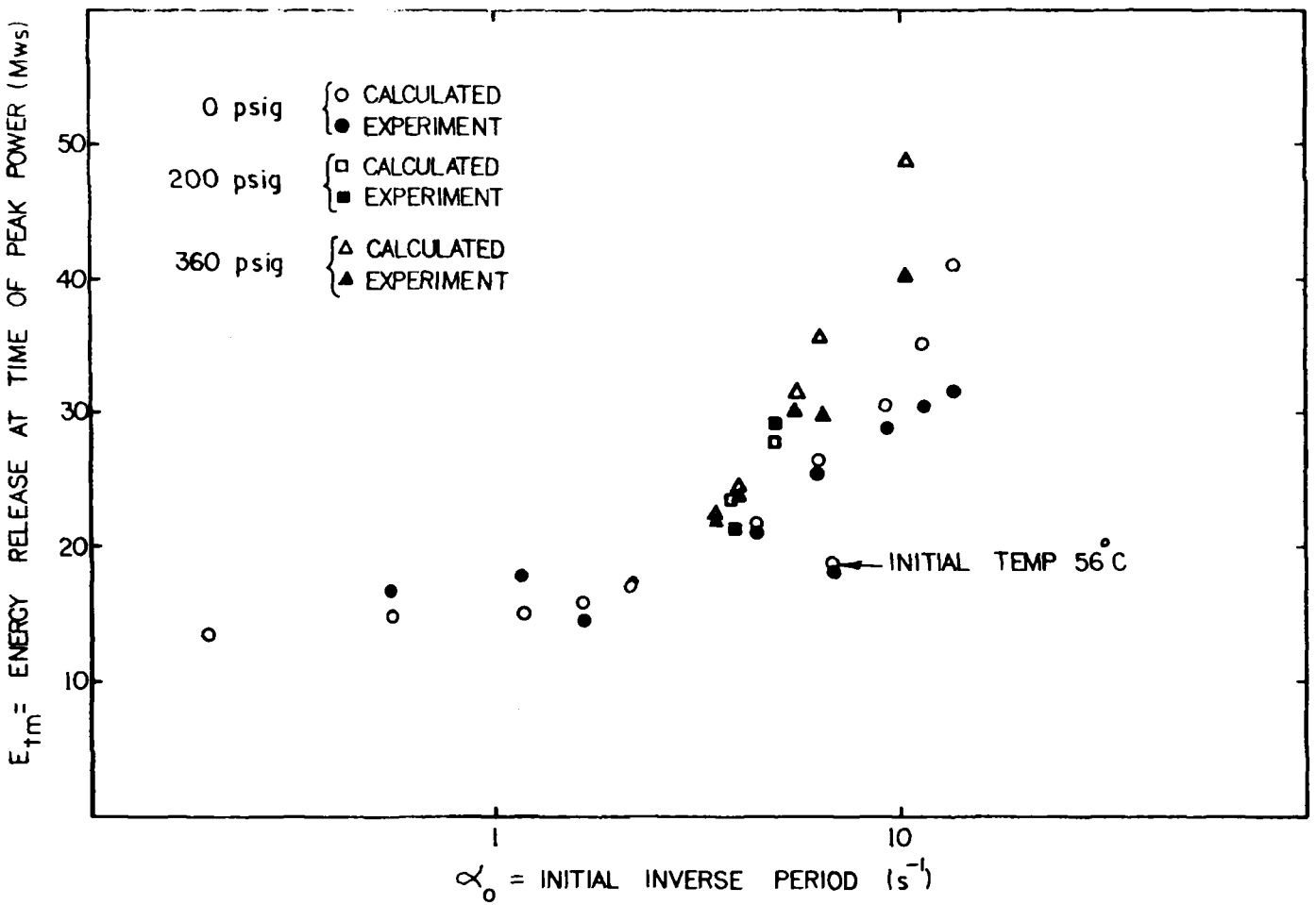

FIG. 2.9 CALCULATED & EXPERIMENTAL ENERGY IN SPERT II CORE B18/68

this arises basically from the assumption that fragmentation of the UO_2 and its dispersal within the sodium coolant can be represented by parameters whose values are independent of the actual heat transfer which follows, the latter being determined purely on the basis of heat conduction between the two materials.

In contrast, the Culham model which assumes that the fragmentation and energy transfer processes are interdependent, predicts that under certain conditions energy can be released with explosive violence. However, although they have demonstrated in small scale laboratory experiments that explosive interactions can occur with water and various molten metals, they have not yet shown this to be the case with LMFBR materials.

Although explosive effects have been demonstrated by experiments in which small quantities of liquid sodium were injected into molten UO_2, e.g. Armstrong (1972) and Anderson and Armstrong (1972), the relevance of these results to an actual reactor environment has been discounted by ANL on the basis that in a reactor excursion the injection of liquid sodium into molten UO_2 is unlikely to occur at any significant level. In addition, the sodium in a reactor channel would contain impurities, such as entrained fission products and gases, thus reducing the probability of high levels of superheating considered necessary to produce the vapour explosion.

Although the results of the TREAT experiments provide some evidence which indicates that explosive interaction between molten UO_2 and sodium is improbable, they do not provide confirmation of the ANL model because in none of the experiments was the mode of mixing of the two materials established. In the absence of this information and in view of the limited number of relevant TREAT experiments, the possibility of explosive interaction cannot be entirely discounted at this stage.

It would therefore appear that in the safety assessment of an LMFBR, the ANL model would not give a comprehensive picture because it excludes a mode of interaction which may possibly lead under certain conditions to a violent explosion. The Culham model, on the other hand, which does include such a mechanism, cannot be applied to the safety assessment of power reactors because it has not been incorporated into a large scale core calculation, nor proved for UO_2/Na systems. The apparent success of the Culham model to date resides only in small scale drop-type experiments. While the initial shock wave set up by a small interaction in a reactor environment can be seen qualitatively to furnish a source of subsequent coherent interaction throughout a region of the core, no quantitative calculations have been reported.

HIFAR Dynamics (D. J. Wilson, J. R. Harries)

HIFAR safety assessments require that power transients resulting from coolant flow changes, such as by failure of a D_2O circulator, can be reliably predicted. This necessitates a satisfactory model for reactivity feedback from thermal effects.

An experiment was carried out in which the temperature of the HIFAR primary D_2O coolant was increased by manipulation of the secondary coolant flow. The consequent power reduction was followed and recorded on magnetic tape. These data are being analysed to devise a suitable model for the thermal feedback of the system.

2.5 MOATA TRANSIENTS (D. B. McCulloch, T. Wall, J. W. Connolly)

Extension of the SPERT transients model (section 2.4) to the MOATA configuration, showed that with static coolant, reactivity transients for initial periods in the ~10 s to ~30 s range would be self limiting at levels below the normal 100 kW full operation power, and would not lead to fuel plate temperature rises greater than about 50°C.

A number of such experimental transients were observed by withdrawal of the calibrated shim rod from its critical setting with the reactor at low power (~10 W). The results are compared with ZAPP calculations in Figure 2.10.

Because the water level in the tanks is significantly lower under static head than with full flow, the power calibration of the reactor installed instrumentation is changed. Although the data displayed in Figure 2.10 correctly related to actual power through an additional counting channel, 100 kW peak power could not be reached without exceeding authorised limits on installed instrumentation. Approval is awaited to extend the experiments to shorter initial periods to approach a true power peak of 100 kW.

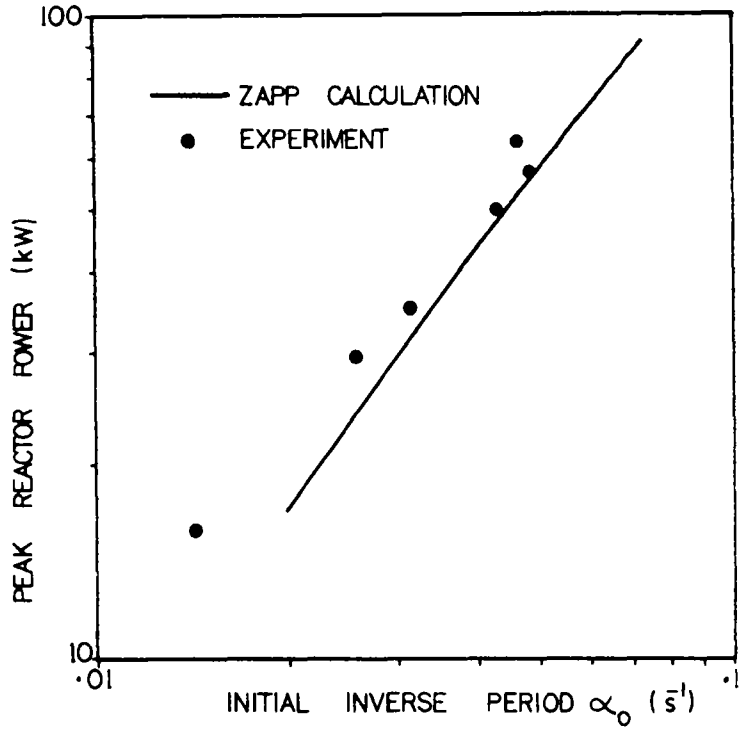

FIG. 2·10 COMPARISON OF 'MOATA' TRANSIENTS WITH 'ZAPP' CALCULATIONS.

2.6 RADIOACTIVE WASTE DISPOSAL (J. R. Harries, D. J. Wilson)

A review of current methods of treatment and storage of high level radioactive waste and the long term options of engineered storage, transmutation and disposal beneath the earth's crust, ice caps, oceans and into space, has been completed. A report of this work, 'The storage and disposal of high-level radioactive waste - a description of current and proposed methods', NSTB PE/6, has been published. The advantages and disadvantages of most of the disposal options are poorly understood. Australia needs to be concerned now about methods that require disposal outside of the country of origin, when any spill of radioactive material would become an international problem. The problems of deep ocean circulation and the transport of radioactive pollutions warrant further study, both because of suggested waste disposal there and also in view of the possible sinking of nuclear propelled ships.

Proposals for high-level waste ocean disposal have required that the waste be contained, possibly in a ceramic matrix, while the waste decays. This is in contrast to the low-level ocean disposal programs which has used dispersal in the vastness of the ocean as the principal disposal mechanism. The isolation of the ocean floor can be illustrated by the estimated residence time of 1200 years for the Pacific Ocean deep water.

A study is being carried out to survey data on the deep ocean circulations in the Tasman and Coral Seas and to relate the water masses in these seas to the world wide ocean circulation patterns. Of particular interest is the vertical transport of pollutants from the deep ocean floor towards the surface, and from the deep water in one ocean to another ocean. It is hoped to be able to estimate the paths and travel times of pollutants being transported from other ocean locations into the Tasman and Coral Seas.

2.7 NEUTRON SOURCE PROJECT (G. R. Hogg, J. Tendys, J. A. Daniel)

A small plasma focus device for operation in the energy range 0.6 to 1.6 kJ (12 to 20 kV) has been constructed and tested. The device is designed to verify the scaling of the neutron yield with stored energy; there is some evidence (Michel et al. 1974)* that the neutron yield per unit energy increases below an energy of 10 kJ. The construction is such that electrode and insulator lengths can be varied and hence the gun can be used over a wide range of pressures and energies. The outer electrode consists of a set of six equispaced rods rather than the solid electrode of the larger device. The inner and outer electrode diameters are 2.5 and 5 cm respectively. Present optimisation experiments indicate satisfactory operation of the device without interelectrode arcing and spurious breakdown under the following conditions: hydrogen gas pressure 6 to 24 Pa (0.05 to 0.2 Torr), applied voltage 18 kV (1.2 kJ), electrode length 10 cm, insulator length 2.7 cm. With deuterium gas fillings, neutron yields of $\sim 10^8$ neutrons per pulse are anticipated. Further optimisation at other operating voltages will be carried out in conjunction with neutron yield determinations.

*Michel, L., Schonbach, K. H., Fischer, H., Applied Physics Letters, 24, 57 (1974).

2.8 NUCLEAR ANALYSIS - PHYSICS

Assaying of Thorium Ores Using Fast Neutrons (A. Rose)

Fast fission in thorium and subsequent counting of the delayed neutrons provides, in principle, a method for determining the concentration of thorium in an ore. In practice, it is difficult to differentiate between neutrons generated by fast fission in thorium from those generated by any uranium that may be in the ore. However, if the uranium content has already been determined by some other technique as, for example, delayed neutron counting after thermal fission in ^{235}U, then the thorium content can be established by subtracting out the uranium contribution.

The 3 MeV Van de Graaff is a suitable source of fast neutrons and operating in a pulsed mode can provide the sequence of irradiation and counting periods necessary to measure the delayed neutrons without physical removal from the irradiation facility required when a reactor is used as the neutron source. The accelerator source can also be tailored to provide a high, fast to slow neutron ratio and to avoid neutrons fast enough to produce delayed neutrons from the ^{17}O reaction.

Preliminary tests using equipment to hand have given some encouraging results. Further investigation is required to reduce the neutron background in the detector system generated during the off-pulse period by the intense source present during the on-pulse period, and to minimise the effect of saturation and the consequent long recovery of the counting system produced during the on-pulse period.

2.9 PULSED NEUTRON TECHNIQUES

Development of Small, Efficient Neutron Detectors (I. Ritchie, S. Whittlestone, E. Clayton)

A need exists in many applications for neutron detectors small in size with high, well defined efficiency for detecting fast neutrons. It is advantageous if such a detector can also be used as a spectrometer to determine the energy spectrum of the neutron field to which it is exposed. Applications include analysis for uranium and thorium in bore holes using delayed fission neutron counting methods, and spectrum measurements carried out inside reactor assemblies. Considerable progress has been made in the development of such a detector based on the hydrogenous scintillators NE213 and NE218, whose pulse characteristics allow good discrimination between incident neutrons and the gamma rays.

Determining the efficiency of the detectors depends crucially on calibrating the pulse height scale of the detector in terms of the energy deposited in the detector by protons generated by neutrons. In the past, it has been usual to do the calibration using gamma rays of well known energy to generate, inside the scintillator, electrons of known energy. The measured relationship between the electron and proton response of the scintillator can then be used to obtain the proton response.

Detector response has been measured using Auger electrons from ^{113}In as a reference source of well-defined energy internal to the detector. This has shown that it is very difficult to relate electron response quantitatively to the pulse height distribution from a monoenergetic gamma ray. In large detectors (~50 mm diameter x 50 mm deep) multiple Compton events blur the Compton edge, while in smaller detectors a high proportion of electrons lose energy in the walls of the scintillator chamber. As well as clarifying interpretation of the shape of gamma ray pulse height spectra, the ^{113}In electron source has permitted evaluation of the positional dependence of light collection efficiency of the scintillator chamber-photomultiplier system. This phenomenon has not been reported before.

It is now possible to measure accurately the two parameters, electron response and space dependent light collection efficiency, needed to calculate the scintillator's response to neutrons. These two parameters have been included in the code used to calculate neutron response functions and it is expected will bring experimental measurements and calculations closer together.

2.10 NEUTRON DETECTION BY ORGANIC SCINTILLATORS

Detector Efficiency Calculations (E. Clayton)

The use of analytic formulae for detection efficiency is now seen to be inadequate and direct numerial calculation is required. Neutron collisions in the detector are simulated by a Monte Carlo code which, given some incident neutron spectrum, calculates a distribution of energy transferred to recoil protons and carbon nuclei in the detector. In an experiment these events cause scintillation, resulting in an output voltage from a photomultiplier. The size of the pulse is a measure of the energy deposited in the detector. This data is revealed as a pulse height spectrum in a multichannel pulse height analyser. In our calculations, this spectrum is simulated by a resolution function acting on the energy distribution. This function incorporates resolution broadening due to the experimental apparatus (photomultiplier statistics, etc.) The resolution function used is that devised by Prescott* which uses light input data to yield a pulse height spectrum.

An efficiency calculation is an 'integral' measure of the fraction of the pulse height spectrum above a certain threshold. The actual shape of the spectrum is largely undetermined by an efficiency measurement. As the pulse height spectrum is calculated in our code, a detailed (channel by channel) comparison has been made with experimental measurement of the pulse height spectra.

Although efficiency calculations are in agreement with other theoretical works, a discrepancy has been found in the high energy region of the spectrum and is thought to arise from two sources. Firstly, the difficulty in calibrating the detector with gamma ray Compton electrons and secondly, a variation in light collection efficiency over the detector. Previous workers have assumed this position dependence is negligible in small detectors, but measurements on small detectors at the AAEC have demonstrated otherwise. The Prescott resolution function has been modified to take this into account and we hope to begin a comparison with experimental measurements in the near future.

---

*Prescott, J. R., NIM 22, 256 (1963).

3.1 3 MeV ACCELERATOR

The accelerator was used for 4201 hours during the year July 1, 1974 to June 30, 1975. Time allocation for the 17 experimental projects is shown in Table 3.1. Maintenance and development accounted for 2228 hours. The only major shutdown during the year was for the replacement of the belt after 13 000 hours of operation. An overhauled accelerating tube has now been in operation for 16 000 hours.

In a development project, measurements were made of terminal power supply voltages under normal running conditions. It was noted that while pulsing and bunching circuits are being used, these voltages drop because of the increased alternator load. Additional fuse protection has also been provided in pulsing circuits to prevent transformer damage. A further four 6A x 4 rectifiers were replaced by silicon diodes.

The interlock and alarm system was modified to allow unattended operation of the accelerator. The system has worked smoothly and has eased the problems of out-of-hours running.

Beams of helium ions have been accelerated and a beam profile monitor has been installed to enable easier beam alignment.

ON-LINE COMPUTER SECTION

CAMAC

In 1973 it was decided to adopt the international CAMAC standard for interfacing additional instruments to the accelerator data acquisition facility. While CAMAC modules are standard, the connection of the CAMAC crate to a specific computer requires a special interface. It was decided to construct a simple interface for connecting up to 7 crates to the PDP-15 using the EUR 4600 convention. For each crate (characterised by crate number C) there are 23 module stations (N) each containing up to 16 sub-addresses (A) and responding to 32 function codes (F).

A total of 17 bits of CNAF code are therefore required to specify an operation and this cannot be conveniently supplied using the ordinary I/O instructions for the PDP-15. Since, however, 18 bits of memory address are supplied by the PDP-15, through the use of an index register it was decided to address CAMAC devices as memory, in a fashion analogous to the PDP-11 unibus principle. A special interface was constructed for the memory bus of the PDP-15. The interface has been installed and works for most operations.

TABLE 3.1

ACCELERATOR TIME ALLOCATION - JULY 1, 1974 TO JUNE 30, 1975

Topic	Experiment Title	Personnel	Origin	Running Time (hours)
Neutron Data				
1. Fission	$\bar{\nu}$ versus E_n	Boldeman, Walsh	Physics	
	Fragment Angular Distribution	Caruana	Wollongong	
	^{252}Cf	Culley	Physics	1648
2. Capture	Capture Gamma Ray Spectra	Kenny, Allen	Physics	
		Barrett, Bray, Joye	ANU	
	Capture Cross Sections	Pe, Allen, Kenny	UNSW/Physics	678
Neutron Transport	Pulsed Integral - Thorium	Rainbow	Physics	
	Pulsed Spectra - Thorium	Whittlestone	Physics	
	Spectra - Fast Assemblies	Rose	Physics	424
Elemental Analysis	Oxygen Analysis	Bird, Russell	Physics	
		Murch	Flinders	
	Scanning	Scott	Physics	154
Independent AINSE Projects	Proton and Helium Channelling	Szpitalah, Kelly	UNSW	217
	Crystal Irradiation	Anderson, Pollard	UNSW	302
	(p,γ) Spectroscopy	Mya, Solomon, Paire	Melbourne	523
	Element Analysis	Atkinson	Melbourne	153
	^{13}N Production	Nicholas	Adelaide	32
Open Day Demonstration			Physics	22
Tests			Physics	48

Total operating time	4201 hours
Maintenance and development	2228 hours
Unused time	2327 hours

Some timing problems were resolved by minor modifications to the PDP-15 processor.

The following CAMAC modules are now available:

- One teletype interface BI-RA 6711
- One quad analog voltage output module (Elliott 1040 DAC)
- Two ADV interface modules (Nuclear Enterprises 7060)

The ADC interface modules have been adapted to suit the existing CI 8060 and ND 2200 ADCs with provision (as yet untested) for joint multi-parameter operation.

PDP-15 Operating System Software

The PDP-15 software has been reorganised to run under the control of an I/O and task supervisor CAMON, which allows for the forthcoming core expansion. An assembler has been written (in IBM 360 assembler language) to enable multiple page and/or bank programs to be assembled for the PDP-15 to utilise the additional memory. Programs currently available which operate under CAMON are CAMS, CAMPHA and HAMPSTER.

CAMS is a PDP-15 program which initiates and responds to interactive link tasks in the IBM 360 via the site DATAWAY. This program also allows access to the IBM 360 HASP internal console and can simulate a printer for batch job output on the PDP-15's teletype.

CAMPHA and HAMPSTER are pulse height analysis programs which can dump or retrieve spectra from paper tape or the DATAWAY. HAMPSTER offers the additional feature of spectrum stabilisation.

PDP-11

A multi-parameter program was written for the PDP-11 used in fission studies to record data event by event on either magnetic tape or paper tape output. Pulse height spectra corresponding to nominated parameters are built up and stored in the computer for display during a run. The problem takes its data input from an existing multiple event data sequencer programmer and can, in principle, cater for 21 simultaneous data sources. It was hoped that using the computer to write the magnetic tape output would eliminate data errors which were previously associated with the recording technique. However, serious hardware problems have been encountered with the magnetic tape unit itself.

Spectrum Stabilisation

A PDP-15 program has been developed to detect spectrum shifts and apply zero and gain correction voltages to the ADC. The program HAMPSTER employs a 'post storage' inspection of the spectrum data, scanned after each display sweep. Two peaks are employed, one of which is assumed to reflect only zero shifts (low energy) and the other mainly gain shifts (high energy). Both peaks are scanned in turn by a common routine which adjusts the output of the digital to analog converter.

Two windows are defined for each peak and the summed counts for each window are stored when a correction is made. On each scan, the new sum is calculated and compared with the old to determine the recent increment to each window. If the recent increments differ by more than a specified number, the output voltage is adjusted by one unit in the appropriate direction, regardless of the magnitude of the discrepancy. If the sum of the recent increments reaches a specified value before a correction is called for, the 'old' window contents are updated anyway.

The stabilisation parameters are entered using the teletype command SSC P_Z, W_Z, D_Z, S_Z, P_G, W_G, D_G, S_G

where P_Z = centroid of lower peak,
W_Z = width of each window,
D_Z = differential count before correction,
S_Z = summed count before resetting differential.

P_G, W_G, D_G, S_G are as above for higher peak.

Results

For testing purposes, a third CAMAC digital to analog converter was used to drive a chart recorder, giving the value of the most recently adjusted correction signal. Simultaneous plots of zero and gain correction over week-end runs were thus compared with control room temperature recordings over the same period. Corresponding to cyclic temperature variations of $\approx 1.5^{\circ}C$, correlated gain correction equivalent to ≈ 2 channels were observed. Zero corrections corresponded to less than 0.5 channels.

Computer Maintenance

Repair of faults in the PDP-7 and PDP-15 computers required 12 and 5 days respectively in the 12 month period.

3.2 FISSION STUDIES (J. Boldeman, J. Caruana, D. Culley, R. Walsh)

Energy Dependence of $\bar{\nu}_p$ for ^{230}Th, ^{232}Th and ^{231}Pa

A series of measurements are in progress to test a hypothesis concerning the dynamics of fission. In a recent study of the ^{240}Pu fission system, Lachkar et al.* have shown that the data are consistent with two modes of fission - the first for sub-barrier fission is superfluid whereas for above barrier fission damping occurs in the latter stages of the process. A prediction of the model is that $\bar{\nu}_p$ behaviour for sub-barrier and above barrier fission should be significantly different. To date, $\bar{\nu}_p$ values for neutron fission of ^{232}Th have been obtained for the energy range 1.3 to 2.0 MeV.

Fine Structure in $\bar{\nu}$ for ^{233}U, ^{235}U and ^{239}Pu

The question of fine structure in the variation of $\bar{\nu}_p$ of ^{233}U, ^{235}U and ^{239}Pu for low energy neutron fission has never been satisfactorily resolved. Our own studies have shown:

1. Linear behaviour for ^{239}Pu in agreement with most other experimental investigations.
2. Clear non-linearity for ^{233}U with which other earlier measurements are consistent.
3. Linear behaviour for ^{235}U which is in disagreement with the majority of other measurements.

To clarify the situation, channel analysis of the fission cross sections for ^{233}U and ^{235}U has been carried out. The partial fission cross sections calculated as in section 4.4 have been used. Furthermore, it has been assumed that the collective energy at the saddle point is only weakly coupled to the nuclear degrees of freedom at scission. Thus $\bar{\nu}_p$ and $\bar{E}_K$ (variation of the average total fission fragment kinetic energy) should reflect the variation of the average saddle point collective energy. The calculated $\bar{E}_K$ behaviour for ^{233}U and ^{235}U are shown in Figures 3.1 and 3.2 respectively, together with the experimental data. It is observed that the calculated dependence reproduces quantitatively the measured non-linearity for ^{233}U whereas the calculated behaviour for ^{235}U supports our linear dependence.

---

*Lachkar, J. et al., Int. Symp on Neutron Induced Reactions, Smolenice, 1974.

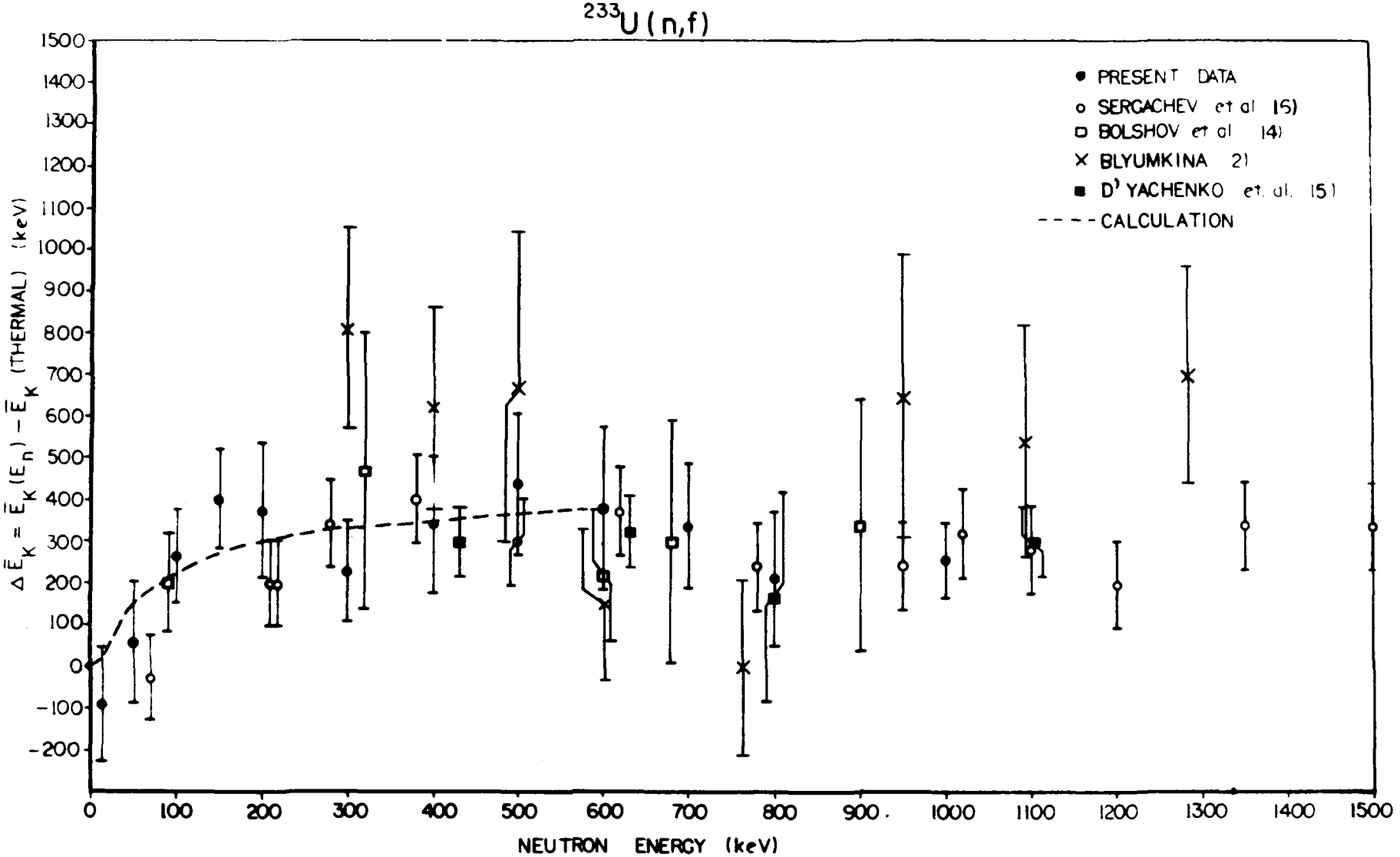

Figure 3.1 Average total kinetic energy as function of incident neutron energy for fission of ^{233}U

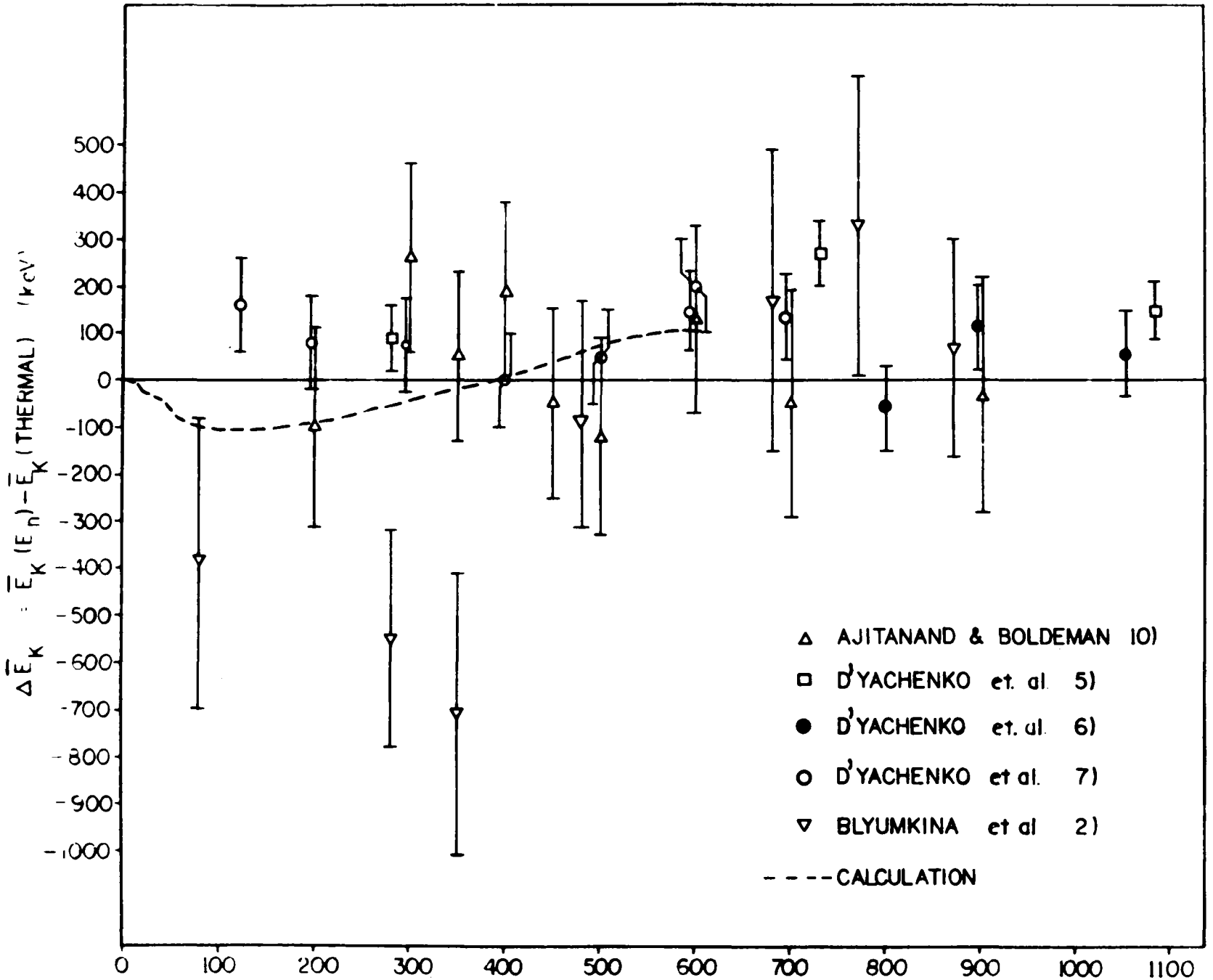

Figure 3.2 Average total kinetic energy as function of incident neutron energy for fission of ^{235}U

Neutron Emission from Specific Fission Fragments

Hardware problems with the magnetic tape system have still not been overcome. To circumvent the problem, a fast paper punch has been interfaced to the PDP-11. To confirm previously observed even-odd effects in the neutron emission per fragment versus fragment mass curve, the earlier measurements on the spontaneous fission of ^{252}Cf have been repeated. Data from approximately 5×10^6 fissions have been stored and analysis is proceeding.

Angular Distribution of Fission Fragments from Neutron Fission of ^{233}U, ^{235}U and ^{232}Th

A systematic error has been uncovered in the earlier fission fragment angular distribution studies for neutron fission of ^{233}U and ^{235}U. Consequently, the measurements have been repeated. In addition, they have been extended to include neutron fission of ^{232}Th.

3.3 FISSION MEASUREMENTS

Time of Flight Measurement of ^{252}Cf Fission Neutron Spectrum (D. Culley)

The time resolution of the plastic (NE102A) neutron detectors has been measured using a gamma-gamma coincidence technique with a ^{60}Co source. The FWHM is 507 ps for both detectors, giving an FWHM of 358 ps per detector.

The 'neutron telescope', which will be used to determine the absolute efficiency of the neutron detectors has been exhaustively leak tested and modifications made to improve its continued leak tightness. Gas fillings and operating parameters for the proportional counters of the telescope are being extensively investigated. An IBM 360/65 program is in hand to calculate telescope efficiencies and incorporates corrections necessitated by recent work on anisotropy of the n,p reaction.

The fission detection chamber has been tested with a small (1.66×10^3 fissions s^{-1}) ^{252}Cf source, but problems exist with quenching of the Xenon light signal. Consequently, the chamber is being rebuilt using lead gaskets and Teflon 'O' rings instead of rubber. Some preliminary measurements of the timing resolution of the chamber/neutron detector combination have been made and the FWHM appears to be about 0.6 ns.

3.4 NEUTRON CROSS SECTIONS (M. Bartle, J. Boldeman, A. R. deL. Musgrove)

Absolute Cross Sections

A system to provide absolute neutron fluxes utilising the associated particle method is being established on the 3 MeV Van de Graaff accelerator in collaboration with Dr. M. Bartle (AINSE Fellow, ANU). The system will be used for precision cross section measurements.

Neutron Total Cross Sections

Neutron total cross section data accumulated on 80 and 200 m flight paths at the Oak Ridge Electron Linear Accelerator are being analysed in collaboration with Dr. J. A. Harvey (ORNL). The analysis procedure is now operational and analysis of the data for ^{92}Zr and ^{94}Zr is proceeding. The data obtained will be used as input in the analysis of capture cross section data for ^{92}Zr and ^{94}Zr.

Neutron Capture Cross Sections (B. J. Allen, J. W. Boldeman, M. J. Kenny, A. R. deL. Musgrove)

High resolution capture cross section data measured at the Oak Ridge Electron Linear Accelerator in collaboration with R. L. Macklin (ORNL) are being analysed at Lucas Heights to obtain results meeting high priority requests from reactor development programs and assisting in the interpretation of measurements made at Lucas Heights.

Neutron Capture Cross Section of Natural Silicon

The neutron capture cross section of natural silicon has been analysed for energies up to 1500 keV. Complete resonance data has been obtained for most resonances in ^{28}Si, but only values of $(g\Gamma_n\Gamma_\gamma/\Gamma)$ have been obtained for neutron capture resonances in ^{29}Si and ^{30}Si. A strong positive correlation is observed between the radiative width and the reduced neutron width for p-wave resonances in ^{28}Si, confirming significant valence effects. It was not possible to confirm from the present measurements a reported asymmetry observed in two resonances in the $^{29}Si(\gamma,n)$ reaction.

Resonant Neutron Capture in ^{40}Ca

The neutron capture cross sections of ^{40}Ca has been measured with high resolution ($\Delta E/E \approx 0.2$ per cent) and resonance parameters obtained for resonances below $E_n = 300$ keV.

The average resonance parameters obtained from the data are as follows:

$\langle D \rangle$ = 37±4 keV, $10^4 S_1$ = 0.16±0.05, $10^4 S_2$ = 2.0±0.7. The average radiative widths and standard deviations of their distributions were found to depend on ℓ as follows: $\langle \Gamma_\gamma \rangle_s$ = 1.5±0.9 eV, $\langle \Gamma_\gamma \rangle_p$ = 0.36±0.09 eV and $\langle \Gamma_\gamma \rangle_d$ = 0.74±0.36 eV.

Odd-Even Effects in Radiative Capture in ^{42,43,44}Ca EXF 30356

The neutron capture cross sections of ^{42,43,44}Ca have been analysed and resonance parameters obtained for energies up to 230 keV in ^{42}Ca, 40 keV in ^{43}Ca and 165 keV in ^{44}Ca.

The average resonance parameters obtained are as follows: $\langle D \rangle$ = 8.6±1 keV, 1.48±0.2 keV and 16±2 keV for ^{42,43,44}Ca respectively. The s-wave neutron strength functions were found to be $10^4 S_0$ = 2.7±0.3, 3.1±0.3 and 2.0±0.5 for ^{42,43,44}Ca respectively.

The s-wave radiative widths for the even-A isotopes were found to be considerably greater than for ^{43}Ca. An explanation in terms of a pygmy dipole resonance near threshold has been suggested. In addition, p-wave radiative widths in the even-A isotopes are anomalously small.

Neutron Capture in Chromium Isotopes (^{50}Cr, ^{52}Cr, ^{54}Cr) EXF

Analysis of the ORELA data for these isotopes has been completed and the results are to be compared with those obtained with a ^{Nat}Cr sample. In ^{50}Cr, 55 resonances were analysed in the neutron energy range 5 to 200 keV and in ^{52}Cr, 50 resonances were analysed in the neutron energy range 5 to 350 keV. In ^{54}Cr only 9 resonances were observed for energies up to 120 keV and 4 resonances observed above that energy. Table 3.2 lists resonance parameters observed in ^{50}Cr(n,γ). Prompt background effects in the capture detector prhibit a definitive analysis of the 5.64 keV resonance in ^{50}Cr.

^{56}Fe Neutron Capture Cross Section

The capture yield from enriched ^{56}Fe has been measured by R. L. Macklin (Oak Ridge National Laboratory) and has been analysed up to 232 keV, and resonance parameters are compared to total cross section results in Table 3.3. Sample thickness was 0.041 atoms per barn.

keV Neutron Capture Cross Sections of ^{134}Ba and ^{136}Ba EXF. 30328

The neutron capture cross sections of ^{134}Ba and ^{136}Ba have been analysed in the energy region 3 to 100 keV. The following average quantities were

deduced from the extracted resonance parameters: $\langle D \rangle$ = 127±10 eV, $10^4 S_0$ = 0.85±0.3, $10^4 S_1$ = 0.8, $\langle \Gamma_\gamma \rangle$ = 120±20 meV for ^{134}Ba. Analysis of the ^{136}Ba data gave $\langle \Gamma_\gamma \rangle$ = 125±30 meV for s-wave neutrons.

The average 30 keV capture cross sections for these two s-process nuclei were found to be 225±35 mb for ^{134}Ba and 61±10 mb for ^{136}Ba.

keV Neutron Resonance Capture in ^{137}Ba EKF 30828

The neutron capture cross section of ^{137}Ba has been analysed up to 60 keV and resonance parameters obtained for resonances in the energy region 2.7 to 12 keV.

The average resonance parameters obtained from the present data are as follows: $\langle D \rangle$ = 380±70 eV, $\langle \Gamma_\gamma \rangle$ = (80±15) meV, $10^4 S_0$ = 0.57±0.2, $10^4 S_1$ = 0.45±0.2. The absolute normalisation error of the data was ≤15 per cent. The s-wave radiative width and s-wave neutron strength functions are the lowest among the barium isotopes.

Compilation of 30 keV Maxwellian Averaged Capture Cross Sections

Capture cross section data in the region of 30 keV have been compiled up to January 1975 and incorporated in a computer file. Where resolved resonance capture data are available, they are weighted by the Maxwellian thermal distribution for kT = 30 keV. Results for even and odd Z isotopes are shown in Figure 3.3. These data are of value for fission product nucleosynthesis applications.

TABLE 3.2

RESONANCE NEUTRON CAPTURE IN ^{50}Cr (9 to 202 keV)

Resonance Energy (keV)	$g\Gamma_n\Gamma_\gamma/\Gamma$	Area (beV)	ℓ	g_J	Γ_n (eV)	Γ_γ (meV)
9.325	0.033	14.9	2	3.0	0.011	1111
18.675	0.431	98.3	1	1.67	10.0	265
19.275	0.294	64.9	1	1.67	10.0	179
24.13	0.027	4.7	2	3.0	0	500
24.94	0.228	39.0	1	1.67	15.0	138
28.55	0.324	48.3	0	1.0	435.0	324
33.55	0.546	69.3	1	1.67	8.0	341
35.56	0.734	87.8	1	1.67	34.0	445
35.72	0.377	44.9	1	1.67	16.0	229
37.00	2.497	287.3	0	1.0	2117.9	2500
40.74	0.503	52.5	1	1.67	30.0	304
46.86	0.536	48.7	1	1.67	15.0	328
50.20	0.432	36.6	1	1.67	30.0	261
53.75	0.524	41.5	1	1.67	20.0	319
55.15	0.092	7.1	0	1.0	280.0	92
55.32	0.192	14.8	1	1.67	15.0	116
55.70	0.110	8.4	1	1.67	25.0	66
59.35	0.679	48.7	1	1.67	25.0	413
63.42	0.323	21.7	1	1.67	25.0	195
64.97	0.371	24.3	0	1.0	45.0	374
66.02	0.622	40.1	1	1.67	25.0	378
68.42	0.258	16.0	1	1.67	40.0	155
70.50	0.358	21.6	1	1.67	30.0	216
73.52	0.536	31.0	1	1.67	25.0	325
78.02	0.618	33.7	1	1.67	125.0	371
79.26	0.708	38.0	1	1.67	100.0	426
88.90	0.444	21.2	1	1.67	30.0	268
90.56	0.590	28.0	1	1.67	30.0	361

TABLE 3.2 (cont'd)

Resonance Energy (keV)	$g\Gamma_n\Gamma_\gamma/\Gamma$	Area (beV)	ℓ	g_J	Γ_n (eV)	Γ_γ (meV)
95.70	1.564	69.6	0	1.0	2500.0	1565
98.60	1.188	51.3	1	1.67	60.0	720
107.95	0.920	36.3	1	1.67	90.0	554
110.80	0.727	27.9	1	1.67	50.0	439
112.75	1.624	61.3	1	1.67	200.0	977
116.30	0.357	13.1	1	1.67	40.0	215
116.90	0.764	27.8	1	1.67	40.0	463
121.65	0.929	32.5	1	1.67	70.0	561
129.75	0.852	28.0	0	1.00	700.0	853
129.80	0.753	24.7	1	1.67	30.0	458
137.15	1.702	52.8	1	1.67	60.0	1037
140.50	0.579	17.6	1	1.67	60.0	349
141.60	0.662	19.9	1	1.67	60.0	399
142.82	0.931	27.8	1	1.67	60.0	563
147.30	0.705	20.4	1	1.67	60.0	425
150.95	1.973	55.6	1	1.67	120.0	1193
153.40	0.935	25.9	1	1.67	50.0	566
157.20	0.750	20.3	1	1.67	50.0	453
157.30	1.125	30.4	0	1.00	1200.0	1126
162.90	0.752	19.7	1	1.67	350.0	451
169.00	0.234	5.9	1	1.67	20.0	141
169.30	0.370	9.3	0	1.00	300.0	370
177.00	3.106	74.7	0	1.00	1000.0	3116
187.38	2.803	63.7	1	1.67	175.0	1695
202.30	2.410	50.7	1	1.67	100.0	1464

TABLE 3.3

^{56}Fe RESONANCE PARAMETERS

ORELA			d) Pa+75			d) Ho+69	
Capture			Total			Capture	
E_n (keV)	a) Γ_n (eV	$g\Gamma_\gamma\Gamma_n/\Gamma$ (eV)	E_n (eV)	$g\Gamma_n$ (eV)	ℓ	E_n (keV)	$g\Gamma_\gamma\Gamma_n/\Gamma$ (eV)
						1.15	$g\Gamma_n$ = 0.086
						2.35	0.0004
7.217	b) $g\Gamma_n$ = 0.00022						
						11.2	0.043
12.45	b) $g\Gamma_n$ = 0.0018						
17.74	b) $g\Gamma_n$ = 0.016						
20.16	b) $g\Gamma_n$ = 0.0081						
22.77	4	0.25				22.7	0.19
27.7	c)		27.66	1500	0	27.7	Γ_γ = 1.44±0.14 Ho+69
							1.5 ±0.3 MPG64
							1.3 Mo65
							1.4 ±0.2 EFK70
34.19	(3)	0.64				34.1	0.57
36.67	(5)	0.29				36.6	0.30
38.37	(3)	0.38				38.3	0.46
45.98	10	0.43				45.8	0.32
			51.55	0.35			
52.05		0.61	52.12	23.8		51.9	0.51
53.49		0.37	53.54	1.0		53.3	0.54
			55.37	1.9		55.0	0.14
59.14		0.86	59.20	8.1		59.0	0.54
63.37		0.77	63.44	4.6		63.1	

TABLE 3.3 (cont'd)

ORELA			Pa+75			Ho+69
Capture			Total			Capture
E_n (keV)	a) Γ_n (eV)	$g\Gamma_\gamma\Gamma_n/\Gamma$ (eV)	E_n (eV)	$g\Gamma_n$ (eV)	ℓ	E_n (keV)
72.87	20	0.88				72.6
73.98		0.67	73.98	530	0	74.6
76.95		0.28	77.04	3.1		76.7
80.69		1.44	80.80	20		80.4
83.65		1.19	83.65	1300	0	
90.14		0.59	90.29	28		90
92.50	3.2	0.93				
97.75	(10)	0.53	92.65	3.2		(92.1)
96.10	80	1.26	96.14	2.0		(95.9)
			96.29	1.3		
96.44		1.05	96.57	5.0		
102.5	70	0.63	102.63	42		(102)
102.9	(10)	0.74				
105.7		1.49	105.87	5.6		
112.5		0.97	112.64	11		(112)
120.8	b) $g\Gamma_n = 0.024$					
122.4	200	0.40	122.71	92		
122.6	25	0.28				
123.9		0.58	124.1	7.5		
124.91		1.08	125.09	19		(124)
129.6		0.91	129.8	600	0	(129)

TABLE 3.3 (cont'd)

ORELA			Pa+75			ORELA			Pa+75		
Capture			Total			Capture			Total		
E_n (keV)	[a] Γ_n (eV)	$g\Gamma_\gamma\Gamma_n/\Gamma$ (eV)	E_n (eV)	$g\Gamma_n$ (eV)	ℓ	E_n (keV)	[a] Γ_n (eV)	$g\Gamma_\gamma\Gamma_n/\Gamma$ (eV)	E_n (eV)	$g\Gamma_n$ (eV)	ℓ
130.0	(20)	0.98				192.5		1.18	192.9	40	
140.3	2500	2.3	140.4	2800	0	195.3		0.71	195.6	66	
141.1	(30)	0.68				201.1		1.95	201.4	48	
142.2	(30)	0.71				205.4	(250)	1.45			
143.4	[b] $g\Gamma_n$ =	0.084				207.5		1.19	207.8	22	
149.6	40	0.29									
161.3		1.14	161.6	13		208.5	(50)	0.27			
168.80	1500±500	1.07	169.2	1000	0	209.5	(20)	0.39			
168.8		2.00	169.3	10		210.2		1.33	210.5	18	
172.9	240	0.56				215.2	(50)	0.40			
173.4		0.36	173.6	83		220.0		2.16	220.5	990	0
179.3		0.56	179.6	13		221.2		0.64	221.6	15	
180.8		3.26	181.0	51		222.2	(50)	0.22			
			182.3	6		223.1	(15)	1.32			
186.7		0.60	187.0	5		225.2		1.00	225.6	56	
187.6		2.98	187.6	3700	0	229.3		0.62	231.0	15	
189.5		1.08	189.9	30		231.9		2.55	232.3	40	

[a] The Γ_n used to calculate the self shielding correction is normally equal to that given by the total measurement unless that value is inconsistent with the shape fit to the capture data. In these cases the neutron width is quoted. Bracketed values are assumed.

[b] Γ_γ = 1 eV assumed.

[c] Analysis inaccurate because of large multiple scattering and prompt background corrections.

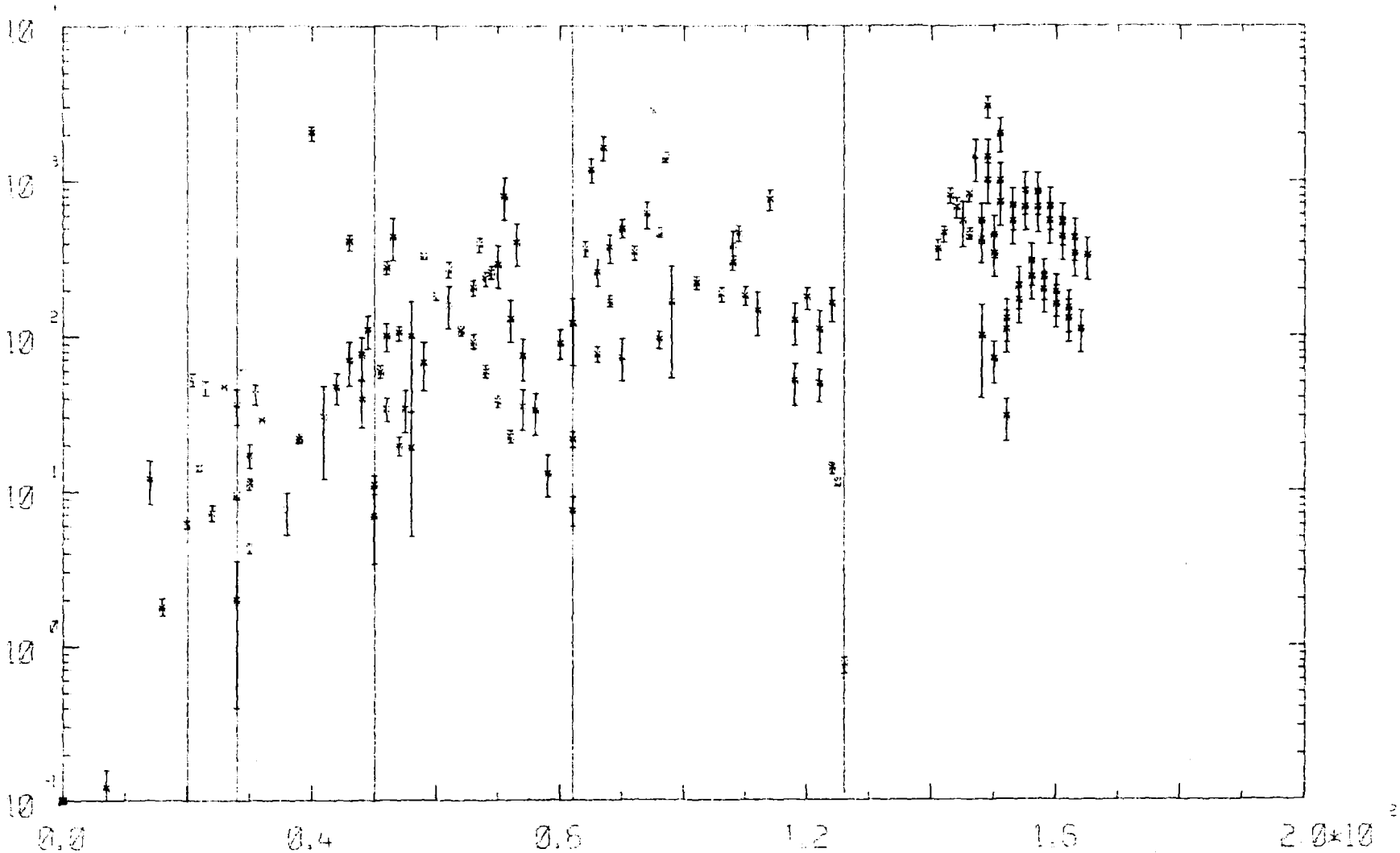

Figure 3.3a Maxwellian (kT = 30 keV) average capture cross sections for even-Z nuclei

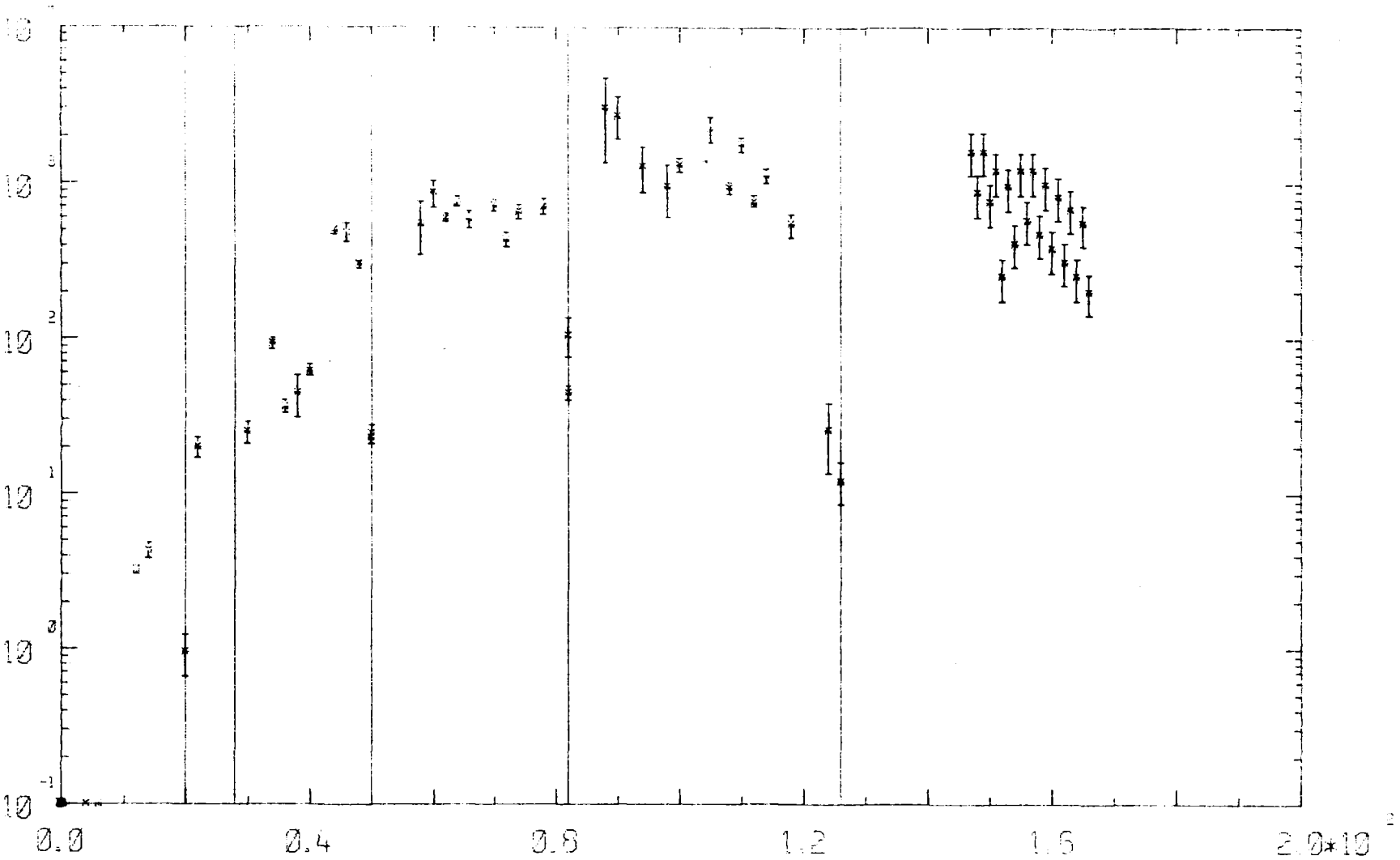

Figure 3.3b Maxwellian (kT = 30 keV) average capture cross sections for odd-Z nuclei

3.5 NEUTRON CAPTURE GAMMA RAYS (Hla Pe, M. J. Kenny, A. R. Joye, K. H. Bray, J. R. Bird, R. F. Barrett, B. J. Allen)

Resonance Neutron Capture Gamma Rays in Silicon

Gamma ray spectra from neutron capture by natural silicon have been measured for resonances at 31.7, 38.8, 55.6 and 67.7 keV. Absolute partial radiative widths have been obtained using the 35 keV s-wave resonance in aluminium as a standard. Strong single particle effects have been observed, although valence transitions are found to be small for these resonances.

It is apparent that these neutron capture mechanisms occur in Si. Direct capture accounts for thermal neutron spectra while the valence model explains the radiative widths of resonances with larger neutron widths. A third mechanism of single particle character, independent of the neutron width, also occurs and is observed in p-wave resonances with small neutron widths.

Radiative Width of 35 keV resonance in ^{27}Al

The radiative width of the 35 keV s-wave resonance in aluminium has been measured relative to the gold cross section using two Moxon-Rae detectors. A value of Γ_γ = (2.2±0.2) eV has been obtained.

The partial radiative width of the ground state transition has been deduced as $\Gamma_{\gamma 0}$ = (1.5±0.3) eV using as the branching ratio for this transition (0.66±0.06) and the evaluated total radiative width. This value is the mean of that obtained with an NaI detector (0.60±0.06) and a re-analysis of recent Ge(Li) data (0.72±0.07).

Non-Statistical Effects in Gamma Ray Spectra Following 0.4 to 1 MeV Neutron Capture

A search for non-statistical effects in the γ-decay spectra following neutron capture has been made for incident neutron energies in the range 40 keV to 1 MeV. The experiments were performed using a 20 cm x 15 cm NaI detector and thirty elements in the range from calcium to uranium were examined. Marked non-statistical effects were found in the spectra from elements in the mass range A=40-70 and in the region around thallium (A=205). The former mass region was explored in some detail. It was found that most results from this regions could be explained in terms of enhanced transition strengths to final states having a strong single particle nature.

In capture γ-ray spectra from the $^{40}Ca(n,\gamma)$ reaction, d-wave capture followed by E1 transitions to the ground state of ^{41}Ca has been observed. Both the statistical and valence models underestimate the measured strengths.

A significant fraction of the total s-wave dipole strength is found to remain in the threshold region, but substantial depletion to the giant dipole resonance occurs for $d_{5/2}$ capture.

Fast neutron capture γ-ray spectra in ^{45}Sc, ^{85}Rb and ^{139}La exhibit anomalous intensities to low lying states with large neutron angular momenta. As the statistical and valence models cannot adequately account for the observed spectra, a capture mechanism based on the formation of two-particle one-hole states is proposed.

Ge(Li) Detector

The efficiency curve of a large volume (21 per cent) Ge(Li) detector as a function of γ-ray energy is being obtained by measuring branching ratios for various resonances in the reaction $^{27}Al(p,\gamma)^{28}Si$ and by comparing intensities from the reaction $^{14}N(n,\gamma)^{15}N$ with well known values. Difficulty in obtaining reproducible peak areas has been experienced because of marked changes in the height of the continuance above and below double escape peaks.

3.6 PROMPT NUCLEAR ANALYSIS (L. H. Russell, A. van Heugten, J. R. Bird)

Characterisation of Obsidian

Measurement of the prompt gamma-rays produced by proton irradiation of obsidian has been found to be a rapid, non-destructive method for deciding the origin of obsidian samples*. This technique has been developed further for the study of South West Pacific obsidian.

A 2.5 MeV proton beam is collimated to 2 or 4 mm diameter and used to irradiate an obsidian sample in an evacuated target chamber. A Ge(Li) detector *7 per cent efficiency for ^{60}Co γ-rays) is placed outside the chamber at 90^{o} to the incident beam. The γ-rays observed are listed in Table 3.4 with the integrated peak counts for an exposure of 250 μC ($\frac{1}{2}$ μA beam for 500 s). The peak areas are obtained from automated computer processing of the γ-ray spectra. Additional small γ-ray peaks are observed, but these have limited application.

Many samples are mounted on a special holder and held in place with copper wire. The sample holder is located by a rod sliding through a vacuum seal. Samples of various sizes and shapes can be used without any special mounting or treatment other than washing to remove surface contamination.

Results for a number of samples from different sources in the South West Pacific are shown in Figure 3.4. In these measurements, 3 mm of Pb was used as a filter to reduce the count rate from the low energy γ-rays. The ratio Al(1013 keV)/Na(440 keV) is plotted against FSUM/Na(440 keV) (FSUM being the sum of counts from the high energy fluorine γ-rays - from 5.0 to 7.2 MeV).

Statistical errors are comparable with the size of the dots in Figure 3.4 but estimated systematic errors arising from many experimental factors are indicated in a few cases by vertical and horizontal error bars.

Measurements on obsidian artefacts are illustrated by the open circles in Figure 3.4 which are results for ten different positions on an obsidian dagger having marked variations in surface condition. These results clearly characterise the dagger as being from Lou Island in the Admiralty group.

---

*Coote, G. E., Whitehead, N. Z., McCallum, G. J. (1972) - Radioanal. Chem. 12, 491.

TABLE 3.4

GAMMA RAYS FROM PROTON IRRADIATION OF OBSIDIAN

(E_p = 2.5 MeV, I_p = 0.5 μA, t = 500 s)

E_γ (MeV)	Reaction	Counts
0.110	$^{19}F(p,p'\gamma)$	33276
0.170	$^{27}Al(p,p'\gamma)$	59873
0.198	$^{19}F(p,p'\gamma)$	34357
0.440	$^{23}Na(p,p'\gamma)$	214760
0.511	Annihilation	13155
0.843	$^{27}Al(p,p'\gamma)$	7093
1.013	$^{27}Al(p,p'\gamma)$	12066
1.630	$^{23}Na(p,\alpha\gamma)$	23146
5-7.2	$^{19}F(p,\alpha\gamma)$	39457

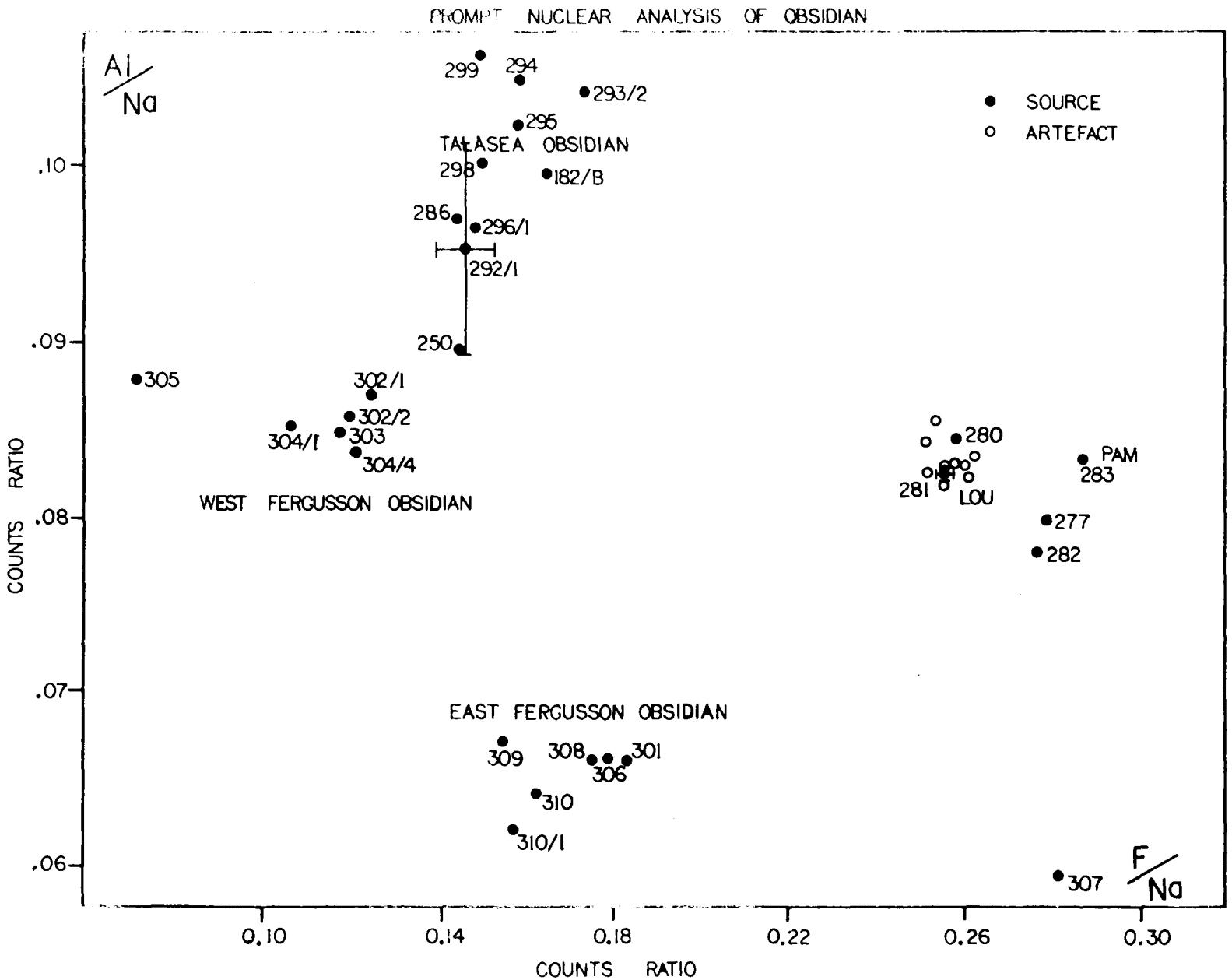

Figure 3.4: Proton induced γ-ray activity ratios for elements in obsidian. Prospects for source identification.

Oxygen Determination

Further measurements have been made of oxygen depth profiles in metals and oxides using the $^{18}O/(p,\gamma)^{15}N$ reaction. These have included tests of the change in alpha particle energy spectrum from changes in detector angle, sample angle and proton beam energy (in the neighbourhood of the 0.846 MeV resonance). Various methods have also been tested for obtaining an increased count rate from low oxygen samples. Typical spectra are shown in Figure 3.5 for a thick oxide of zirconium and a thin layer of oxygen on the surface of semi-conductor grade germanium. The latter spectrum shows counts from surface contamination by boron which sets a lower limit to the sensitivity for oxygen determination.

Further measurements have also been made using gamma rays from reactions in ^{16}O, ^{17}O and ^{18}O for simultaneous measurements of isotope ratio and absolute calibration of both the alpha and gamma methods for oxygen determination.

Neutron Capture Analysis

Increased neutron beam intensity has been obtained by installation of a tapered collimator in the MOATA reactor. Stabilisation techniques have been developed so that standard conditions can be obtained for measurements of thermal neutron capture gamma rays as applied to sample analysis over extended periods. A large Ge(Li) detector (21 per cent efficiency for ^{60}Co gamma rays) is being calibrated and thermal capture results evaluated to provide improved countrate and accuracy in determination of sample composition.

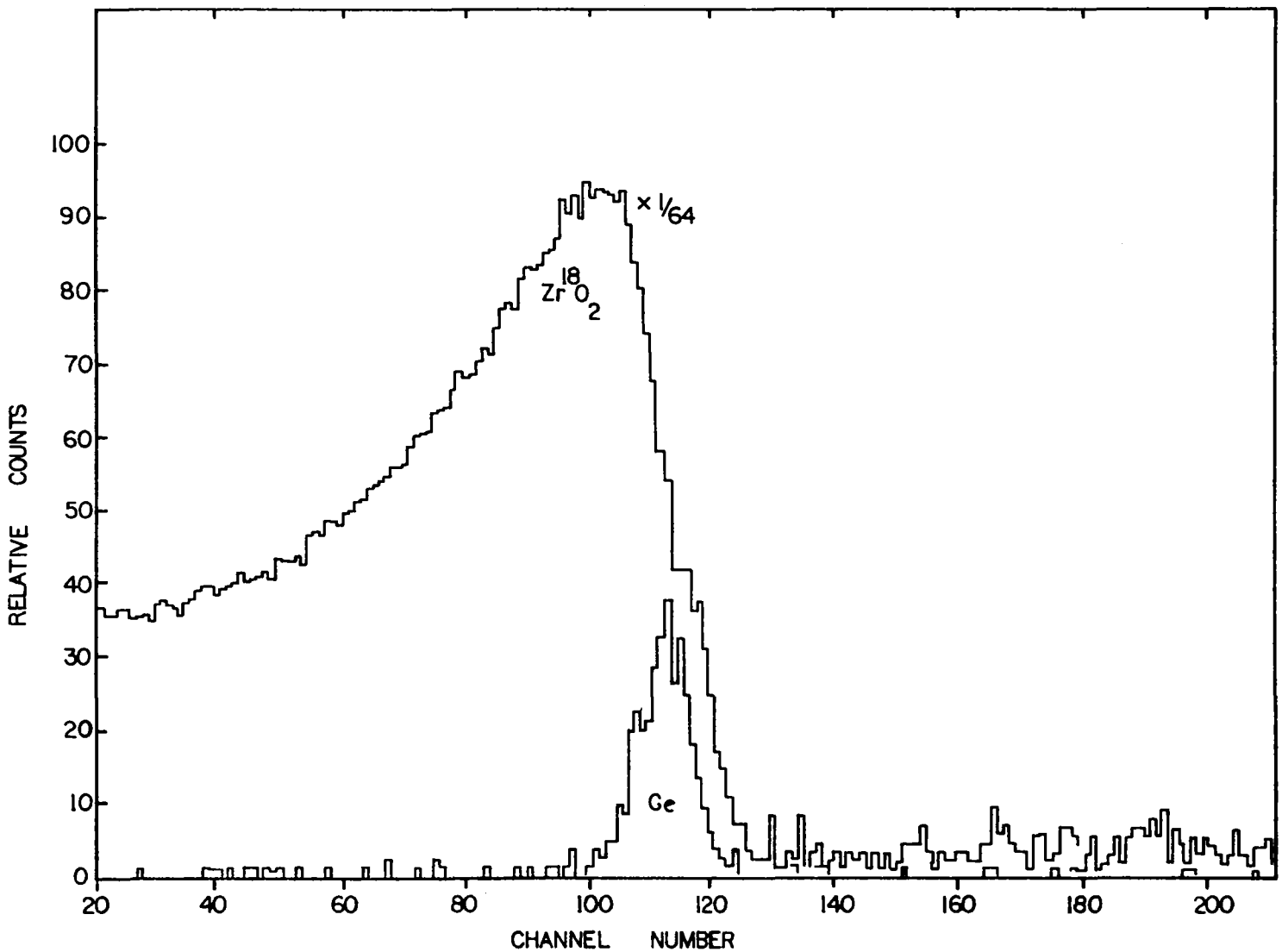

Figure 3.5: Alpha spectra from proton irradiation of zirconium oxide and germanium metal using the $^{18}O(p,\alpha)^{15}N$ reaction

4.1 THEORETICAL PHYSICS

AUS Modular Scheme (B. Clancy, B. Harrington, J. Pollard, G. Robinson)

Checkout of the AUS suite of modules used for reactor calculations continued. In particular, several benchmark type 1 and 2 dimensional kinetics calculations were undertaken with the diffusion module POW.

The work of inclusion of ENDF/B (3 and 4) data into the AUS cross section and kinetics data pools has continued.

AUS Module EDIT

A new EDIT module is being written which will be able to 'unscramble' a succession of smearing and group collapsing operations to give, for example, the fissions due to ^{235}U in a particular part of a reactor undergoing burnup. The user supplies very little additional data as EDIT uses all the data of nuclide concentrations, smearing and group collapsing factors, etc. accumulated during the running of the job and held in the STATUS data pool.

AUS Module MIRANDA

The availability of ENDF/B cross section data has allowed the improvement of certain aspects of the MIRANDA resonance treatment. For nuclides with substantial resonance scattering cross sections, the group transfer scattering cross sections and group transport cross section have a resonance self-shielding component included along similar lines to the treatment of fuel nuclides.

A cluster geometry collision probability routine which involves repeated cylindrical calculations by the Bonalumi method has been included in MIRANDA. This routine has also been included in the ICPP (general purpose collision probability) module, together with a number of more accurate and slower collision probability routines. The addition of the cluster geometry capability to the AUS scheme has thus been almost completed.

AUS.ENDF/B Cross Section Library

The preparation of an AUS cross section library from ENDF/B data files has progressed to the stage where data for most important nuclides is available and the addition of further nuclides as required is fairly automatic. A number of new programs have been developed to prepare data for fuel nuclides in the resolved and unresolved resonance regions. The methods used in the preparation of the library are summarised below.

The ORNL code SUPERTOG is used to prepare group cross sections for all data apart from resonance cross sections and thermal scattering. SUPERTOG 'printed' output is processed by the STOGAUS program to produce an AUS cross section file. Scattering matrices up to P3 order have been prepared as standard.

Thermal scattering data for moderators (H_2O, D_2O, CH_2, C) have been prepared from ENDF/B tabulations of $S(\alpha,\beta)$ smoothly joined to the slowing down data from SUPERTOG using the MERGER program. Thermal scattering data for other nuclides have been prepared by the AUSGAS program which uses a gas model. All thermal scattering matrices have been limited to P0 and P1 data.

The basic approach to resonance data is to prepare group resonance integrals as a function of potential scattering and temperature, and to fit these resonance integrals with subgroup parameters for use by the MIRANDA module. In the resolved resonance region, point cross sections are generated on an extremely fine mesh interval using the POINTXS1 program to process the single-level or multi-level Breit-Wigner parameters on the ENDF/B files. These cross sections are generated in the form of PEARLS tapes and the PEARLS program was initially used to solve the slowing down equations numerically for homogeneous mixtures of the resonance nuclide and hydrogen to give group resonance integrals. The use of PEARLS proved rather time consuming on a routine basis and it has been replaced by the MINI-PEARLS program which solves the same equations, but is restricted to exactly the required problem and is a factor of 4 faster. Tabulated scattering matrices are produced as well as group resonance integrals. This process is applied to resonance scatterers as well as fuel nuclides.

Some difficulties have been experienced with the fitting of group resonance integrals with subgroup parameters and their subsequent use in MIRANDA. The initial work in this area was performed for ^{238}U data prepared by the British GENEX code, which did not include interference scattering. The λ method has required some modification when interference scattering is included and the accuracy of MIRANDA thus obtained has yet to be established.

Two methods are available in the unresolved resonance region, whose use depends on the accuracy required and the data available. For most nuclides, the approach used in SUPERTOG and MC^2 has been adopted. That is, the resonances integrals are computed from a sum of J functions with a numerical integration over the neutron and fission width distributions being performed. This procedure has been coded in the POINTXS1 program. The major approximations

are in the narrow resonance assumption and in the treatment of the overlap of neighbouring resonances, but the method is adequate for most applications. The alternative approach of generating a sequence of resonances by sampling from the width and spacing distributions and hence preparing point cross sections as in the resolved region, has been applied to ^{238}U only.

The prepared library, AUS.ENDF/B, is now the standard AUS cross section library. It is of 128 groups which are identical to the GYMEA groups, apart from an extra group above 10 MeV (lethargy boundaries of - 0.25 (0.25) 13.75, 13.9 (0.1) 20.5 (0.5) 23.0). The contents of the library are given in Table 4.1 All data which is not ENDF/B3 or ENDF/B4 has been extracted from the GYMEA cross section libraries. The library also includes 41 individual fission products and 1 pseudo fission product from the AAEC fission product library.

TABLE 4.1

AUS.ENDF/B CONTENTS

Nuclide	Data Source†	Subgroup Parameters	Temperatures K	Scattering Order
^{232}Th	ENDF/B4	Yes	300	P3
^{233}Pa	PHF68	Yes	900,300	-
^{232}U	NDXD40	No	-	-
^{233}U	ENDF/B4	No	300	P3
^{234}U	JPGYM767	Yes	900,300	-
^{235}U	ENDF/B4	Yes	900,300	P3
^{236}U	JPGYM767	Yes	900,300	-
^{237}Np	ENDF/B4	No	300	P3
^{238}U	ENDF/B4	Yes	900,300	P3
^{239}Pu	ENDF/B4	Yes	900,300	P3
^{240}Pu	ENDF/B	Yes	900,300	P3
^{241}Pu	ENDF/B4	Yes	900,300	P3
^{242}Pu	ENDF/B4	Yes	900,300	P3
CH_2	ENDF/B3	No	296	P3
H_2O	ENDF/B3	No	296	P3
D_2O	ENDF/B3	No	400,296	P3
C	ENDF/B4	No	296	P3
O	ENDF/B3	No	1200,900,600,296	P3
BeO	NDXD40	No	1200,900,600,300	P0
Na	ENDF/B3	Yes	300	P3
Al	ENDF/B4	No	300	P3
Cr	ENDF/B4	Yes	300	P3
Fe	ENDF/B4	Yes	300	P3
Ni	ENDF/B4	Yes	300	P3
ZIRC2	ENDF/B4	No	300	P3
^{6}Li	AEEW69	No	-	-
^{3}He	AEEW69	No	-	-
^{3}T	NDXD40	No	-	-
^{10}B	ENDF/B4	No	300	P3
N	AEEW69	No	-	-

TABLE 4.1 (cont'd)

Nuclide	Data Source†	Subgroup Parameters	Temperatures K	Scattering Order
F	AEEW69	No	-	-
Cl	AEEW69	No	-	-
Ca	AEEW69	No	-	-
Ti	AEEW69	No	-	-
Mn	ENDF/B4	No	300	P3
Co	NDXD40	No	-	-
Cu	ENDF/B4	No	300	P3
Ga	AEEW69	No	-	-
^{63}Cu	NDXD40	No	-	-
^{107}Ag	BNL66	No	-	-
Cd	AEEW69	No	-	-
^{115}In	BNL66	No	-	-
Ta	AEEW69	No	-	-
W	AEEW69	No	-	-
^{186}W	BNL66PHF	No	-	-
Au	AEEW69	No	-	-
Si	AEEW69	No	-	-

†NOTE: ENDF/B3: ENDF/B version 3 data file
ENDF/B4: ENDF/B version 4 data file
AEEW69 : Winfrith data file 1969
BNL66 : BNL325, 1966
Others : Various old data sources

Comparison of Diffusion, S_N and Monte Carlo Codes (B. McGregor)

Performance of the AUS diffusion theory module POW was compared with that of a Monte Carlo code KENO for the calculation of the planned second Critical Facility configuration, a small C-^{235}U cylindrical core with a graphite reflector. The calculated multiplication factors agreed, but differences of the order of 3 per cent were noted in region averaged group fluxes. A one-dimensional spherical geometry was devised to approximate the cylindrical geometry. Differences similar to those already observed were noted when the region averaged fluxes from a POW calculation were compared with an S_N transport (ANAUSN) calculation for the spherical model. Calculations made with S_N and Monte Carlo codes were in good agreement. The observed flux differences were attributable to the POW code and were consistent with the inherent diffusion theory approximations.

A study of the critical mass and lifetimes of uranium assemblies provided an opportunity to compare the two one dimensional S_N codes, ANISN and ANAUSN, and showed up some deficiencies in both. A suggestion to improve the ANISN method of performing α calculations will be made to the code authors.

Flux Tilt in Symmetric Systems Asymmetrically Disturbed (J. Pollard)

In order to understand the extent of some of the asymmetries arising in the spatial flux distribution from asymmetric absorber insertion in some of the one and two dimensional kinetics calculations, undertaken as part of a checkout of POW, the following relationship was derived

$$T = -pd/\{1-d(1-p)\} \quad , \quad p > -(1-d)/(2d) \quad ,$$

where T = flux tilt indicator

$$= \frac{\nu \text{ fissions in undisturbed half} - \nu \text{ fissions in disturbed half}}{\nu \text{ fissions in undisturbed half} + \nu \text{ fissions in disturbed half}}$$

P = reactivity

$$= \frac{\text{disturbed multiplication} - \text{undisturbed multiplication}}{\text{disturbed multiplication}}$$

and d = dominance ratio

$$= \frac{\text{second highest multiplication eigenvalue}}{\text{undisturbed highest multiplication eigenvalue}}$$

Without the (1-p) factor, the result is that obtained by Wade and Rydin*.

*Wade, D. C. and Rydin, R. A. (1972) in Hetrick, D. K. (Ed.) - Dynamics of Nuclear Systems, Arizona Press.

Although (1-p) is usually close to 1, the neglect of the factor for extreme situations (such as the very loosely coupled reactor reported in the Benchmark Problem Book* with d = 0.99844) can reduce T to as much as half of that calculated above (which agrees with that calculated directly to within a few per cent).

4.2 RADIATION SHIELDING

Shielding Codes (I. J. Donnelly and B. McGregor)

The two prerequisities for a shielding calculation are adequate cross section data and suitable particle transport codes. The cross section data presently available at AAEC have been discussed previously (AAEC/PR40-P, section 4.3). The main transport codes presently in use for shielding calculations at AAEC are now briefly outlined.

ANISN-C (197 version) - A transport theory (S_N method) code which gives an accurate flux evaluation in one-dimensional geometries. The latest version of ANISN has recently been obtained from RSIC. Improvements in this version include a weighted central difference option which enables more accurate flux determination for a given spatial mesh size; this option is of particular value for shielding calculations.

SABINE-3 (1973 version) - A removal-diffusion theory code which calculates neutron and gamma ray fluxes in one-dimensional shield configurations. In many cases, it is appreciably faster than S_N codes (typically by factors up to 10) with comparable accuracy. It has the advantage of containing its own cross section library. The latest version of SABINE has recently been obtained from the NEA Computer Program Library. The code can now be applied to a larger range of problems as the user can input a neutron source spectrum rather than being restricted to a fission spectrum. This version also includes updated cross section libraries.

In addition to these codes, use is made of the AUS system for data processing anf flux calculation.

MORSE, a general purpose Monte Carlo code, is used for problems whose geometry is so complicated that no suitable one-dimensional approximation can be devised.

---

*Argonne National Laboratory (1972) - ANL-7416, Supplement 1.

The Accuracy of the Diffusion Theory Component of Removal-Diffusion Theory (I. J. Donnelly)

The neutron fluxes in five shields consisting of water, concrete, graphite, iron and an iron-water lattice, have been calculated using P_1 theory, diffusion theory with the usual transport correction for anisotropic scattering (DT) and diffusion theory with a diagonal transport correction (DDT). The calculations have been repeated using transport theory for the flux above 0.5 MeV and the diffusion theories for lower energies. Comparison with transport theory reveals the accuracy of the diffusion theories for flux evaluation at all energies and for flux evaluation below 0.5 MeV given the correct flux above 0.5 MeV. From the results, it is concluded that the diffusion component of removal-diffusion theory has adequate accuracy unless the high energy diffusion flux entering the shield is significantly larger than the removal flux. In general, P_1 and DT are more accurate than DDT and give similar fluxes, except for shields with a large hydrogen content, for which DT is better. Therefore, use of DT in preference to P_1 theory or DDT is recommended.

A Comparison of ANISN and SABINE Shielding Calculations (I. J. Donnelly)

The transport theory code, ANISN, together with the DCC-9 and DCC-23 couples neutron-gamma ray cross section libraries, has been used to evaluate the neutron and gamma ray fluxes in four simple radiation shields. The calculations have been repeated using the removal-diffusion code SABINE, and the three sets of results compared. This comparison allows an assessment of the accuracy of the calculation methods and of the cross section data used. The shields calculated were 120 cm thick slabs consisting of either water, concrete or iron, and a 120 cm lattice consisting of alternating 10 cm slabs of iron and water. A neutron source was assumed at the left hand side of each shield and the resulting neutron and gamma ray fluxes in each shield were calculated; these fluxes were then used to evaluate the neutron and gamma ray biological doses. In the four shields studied, the differences in neutron doses predicted using the three different calculation methods, is less than 30 per cent for attenuations less than a factor of 10^4, and agreement is found to within a factor of 2 for attenuations up to 10^7. The gamma ray doses agree to within 50 per cent of the largest value. The reasonable agreement obtained between the three calculation methods lead to a favourable assessment of the accuracy of each method for such shielding calculations.

Gamma Ray Spectra from Ores (B. McGregor)

Experiments have been performed at the CSIRO Minerals Research Laboratories to find the variation in the gamma ray spectra from an ore body as it is covered by successive layers of overburden. Using water as overburden, the experiments were run for uranium and thorium ores. It is hoped that a method may be devised which would indicate the thickness of overburden present and thereby reveal an important ore body where the surface reading is only just above background.

Calculations of the penetration of gamma rays through a range of materials were carried out in 1954 by Goldstein and Wilkins*. Their moments method calculations produced the build-up factors used in many gamma ray shielding calculations. To analyse the results obtained from the CSIRO experiment, the moments method spectra were interpolated in material and energy and integrated to give the result for an isotropic and mono-directional plane source. Work is continuing, especially on determining the response function of the 7.7 cm x 7.7 cm NaI crystal to allow better comparison of the calculated and measured spectra.

4.3 PULSED NEUTRON AND SPECTRUM MEASUREMENTS

BF_3 Counter Efficiency (B. Harrington)

The efficiency and energy dependence of five groups of BF_3 counters in the photoneutron moderator under construction at the University of Western Australia was analysed. Absorption reaction rates in ^{10}B were calculated for neutrons with initial energies ranging from 1 MeV to 10 MeV. The efficiency of the detector system was found to vary by approximately 30 per cent in that energy range.

Resolution Studies (D. W. Lang)

(a) Pulsed Time of Flight Spectra

The computer program described earlier (AAEC/PR40-P, section 4.4) has been modified to allow exploration for structure with detail as fine as one ninth of a timing channel. Theoretical analysis of conditions for such structure to be significant has been made. There are two conditions to be met. The spectrum may show sharp, narrow resonances in energy and the beam pulse may be, in fact, a series of shorter disconnected pulses. Unless both

---

* Goldstein, H. and Wilkins, J.E. (1954) - Calculations of penetration of gamma rays. NYO-3075.

conditions hold, the folding of a smooth component with a structured component results in a smooth predicted yield and hence no significant repercussions of the fine structure. The actual data give little evidence for fine structure in either component beyond the success reported earlier.

(b) Resolution Matrices obtained by Measurement

The program described earlier (AAEC/PR40-P, section 4.4) has been assembled as a complete module. The effectiveness is still unknown and must await a full test with experimental data.

(c) Proton Recoil Data

Attempts to unfold neutron spectra from a set of experimental recoil proton measurements were unsuccessful. Several program faults were located and removed. Experience was also gained in unfolding a neutron spectrum over an intermediate range when the high energy spectrum is already known. The program was modified to make as much of the matching process as possible automatic. It was found that the computer generated graphs produced by the program gave valuable information about the success of the correction for the high energy neutrons. The discrepancy between data and the predicted yield shows broad structure at low energies if the high energy end is wrong. When the high energy end is adjusted correctly, the structure disappears.

Neutron Flux Determination by Activation Methods (J. Cook, H. Ferguson)

In conjunction with an Isotopes Division project to activate thin metal wires in HIFAR theoretical studies have resumed on this problem, mainly to determine the epithermal flux. A basic 128 group library of 30 nuclide capture and threshold reactions was prepared and trials begun to test the viability of the method of linear least squares to determine a few group spectrum. It was found that initially the choice of lethargy group boundaries was quite critical, but an area method was devised which gave the optimum group boundary structure quite rapidly.

A spline fitting routine was used to fit to the first solution for the flux and the resultant flux was used to group collapse the cross section library to calculate a second guess for the flux. In this way an iteration procedure developed which, however, did not converge in the case of the trial solutions. It was found that the flux shape is the most critical factor in collapsing the library to obtain a satisfactory solution, so an alternative method was devised.

The slopes of the fluxes in each coarse group were taken to be parameters of the fit and an interaction scheme was set up as before, using a non-linear least squares search program. This method is currently undergoing trials and we do not yet know if it will prove satisfactory.

Another method of flux determination under investigation is to commence the calculation with more groups than are required to yield a unique solution, and by gradually reducing the number of coarse groups until they are less in number than the foils activated, converge the results to a unique answer. To date, all of the above methods have been disappointing, leading to unacceptably large errors on the group fluxes and the main problem appears to be in finding a numerical technique which keeps these errors to a minimum.

Three results have emerged. The first is that the choice of energy boundaries for the groups can be critical - a poor choice giving gross errors in the flux estimates. The second result is that even with a good choice of group boundaries, the errors in the calculated broad group fluxes were sensitive to the assumed within-group spectrum shape used to calculate the group average cross section of the detectors. The third result was that the activation of the detectors by the thermal component of the HIFAR flux dominated the observed count rates so much that a low error determination of the epithermal component was not practicable unless cadmium shielded activations were also available.

Further work on the project is continuing.

4.4 REACTOR DATA

Fission Product Cross Sections (J. Cook, H. Ferguson)

Calculations are continuing on those nuclides with unmeasured cross sections with a view to preparing an ENDF/B data library of such nuclides complete with errors. A cross section generating program was written which, by a rejection technique, ensures that the generated cross section has the correct thermal cross section and resonance integral. The statistical distribution of the generated cross sections was examined and appeared in every case to be well fitted by a truncated Gaussian distribution. The program uses statistical region resonance parameters which have been evaluated fully, and allows for errors on these parameters.

It is hoped that eventually we will have a library of such cross sections in the ENDF/B error format which is then to be used to ascertain the error in the reactivity of fast reactors, which results from a lack of knowledge of

these cross sections. About 120 nuclides in all are being treated which were selected on the basis of the size of their yields from fission and keV capture cross sections. Evaluations for about 40 nuclides with measured keV capture cross sections have already been carried out by other workers and these will be used in our computations of reactivities.

Resonance Parameter Analysis

The statistics of fission widths for partially open fission channels were investigated extensively and the theoretical distributions derived were applied to ^{235}U fission widths in which multilevel effects are negligible. Fits were carried out for 1, 2, 3 and 4 channel distributions to both the J=3 and J=4 spin states. It was found that the J=3 state possessed two partly opened channels. However, the theory predicts only one open channel for the J=4 state, whereas we found an excellent fit to the case where three channels are partly open. We suggest that the fission theorists look again to their models to explain the appearance of two additional channels in this state.

The statistics of both fission and neutron widths for ^{233}U are under study. Multilevel effects are of great importance for this nuclide. We have fitted the fission width distributions in the 2+ and 3+ state and found that about six open channels represents the best fit to each state. This is far too many, so a study of multilevel effects was undertaken to see if the apparent number of channels increased with the size of the multilevel interference. This was found to be the case, and a method was devised for removing the multilevel effects to obtain an estimate of the true number of channels open. To date the results indicate that on average two channels open for each J state, providing the best fit. The exact distribution is being fitted to determine the fission widths in the partially open channels, where the two J states have been lumped together.

The neutron width for ^{233}U affords a very poor fit to the Porter-Thomas distribution, even after missing levels have been taken into account. Previous work on the expected distribution of Kapur-Peierls parameters is being applied to see if the serious discrepancy can be explained.

Fission Yield Mass Curves (J. Cook, E. Rose)

The assumption that the fission mass yield curve can be fitted by three asymmetric Gaussians has been investigated for nuclides ranging from ^{209}Bi to ^{258}Fm. Good fits to the distributions were obtained in all cases and, using the special cases of ^{233}U and ^{235}U, the energy dependence of the Gaussian

parameters was ascertained. The resultant parameters obtained from the energy dependent fit were examined extensively to see if any systematic behaviour with charge and mass number existed. Despite prolonged efforts, no accurate laws enabling the prediction of the parameters was found. Attempts were made to predict the fission yield curve of ^{240}Pu, which is of major importance in fast reactors, but the data obtained so far lacks accuracy too much to be used in reactor calculations.

Statistical Theory for Nuclear Cross Sections (W. K. Bertram)

The conventional statistical theory which is based on the single level approximation in the R-matrix formalism, and which has been quite useful in the analyses of the energy averaged reaction cross sections of many nuclei, has always been found inaccurate when applied to reactions involving the fissile heavy nuclei. An attempt was made to improve the accuracy of the statistical theory by using the multilevel R-matrix formalism for its derivation. However, the modified theory was found to contain approximations which violated the important requirement that the S-matrix be unitary. Therefore, investigations into the effects of unitary on the calculation of averaged cross sections have been carried out. Expressions for the cross sections have been derived using the multilevel R-matrix theory. Subsequently, the theory has been used to investigate the reactions of the nuclei ^{233}U and ^{235}U. Cross sections of the (n,f), (n,n') and (n,γ) reactions, as well as the average kinetic energies and the angular anisotropies of the fission fragments have been calculated and were found to be in excellent agreement with experiment. Investigations into the reactions of other fissile nuclei are continuing.

4.5 THE PROPAGATION OF NEUTRON WAVES IN POLYCRYSTALLINE MODERATORS

(K. J. Maher)

Work on the diffusion theory of neutron wave experiments in polycrystalline moderators was finalised*. Attention was concentrated on a detailed prediction and analysis of the high frequency wave experiments in BeO carried out within the Division by Ritchie and Whittlestone† and to a lesser extent, on analysis of the graphite experiments of Takahashi and Sumita††.

---

*Maher, K. J. (1975) - Ph.D. Thesis, University of Wollongong.

†Ritchie, A. I. M. and Whittlestone, S. (1973) - J. Nucl. Energy 27, 335.

††Takahashi, A. and Sumita, K. (1968) - J. Nucl. Sci. and Tech. 5, 137.

The experiments endeavour to measure a complex frequency dependent relaxation length $K(\omega) = \alpha+i\xi$ characteristic of the moderator's neutron diffusion and scattering properties and the assembly size. The determination of a unique system eigenvalue, K, is contingent on the establishment of an asymptotic scalar flux decay mode. $\phi(E,z,t) = \phi_0^{(E)} \exp(-K(\omega)z+i\omega t)$ at distance z well removed from the incident sinusoidal beam.

The historical trend in the analysis of the experiments has been away from direct calculation of the eigenvalue K towards a full determination of the neutron space and energy dependent neutron spectrum. This development was precipitated by the experimental and theoretical discovery that the system can readily be driven above a critical frequency into a non-asymptotic regime characterised by wave interference effects that preclude a unique $K(\omega)$ value. These effects are evident in Figures 4.1 and 4.2 as variations in the BeO $\alpha(z,\omega)$ and $\xi(z,\omega)$ surfaces calculated by the complex arithmetic, multigroup, one-dimensional finite difference diffusion code MYOPIC.

The calculated α and ξ surfaces show progressive non-asymptotic behaviour above a critical frequency $\omega^* \sim 300$ Hz and are in closer accord with experimental measurements than the results of earlier theoretical workers who predicted, in some cases, α surfaces going discontinuously from $+\infty$ to $-\infty$. Earlier theoretical analyses have been overly idealised, assuming a spatially homogeneous semi-infinite moderating assembly. By contrast, in this work a determined attempt has been made to explicity model experimental features shaping the non-asymptotic behaviour of wave propagation in the moderator. It involved calculating the energy dependence of the neutron wave as it progressively passed from the fast neutron sinusoidal source, through a pre-thermalising tank, and then through a cadmium shutter before entering the moderator. Special low energy neutron cross section libraries were devised to give due weight to the build-up of very low energy neutron populations which are responsible for the wave interference effects observed. Care was taken to process (least squares fitting, etc.) the results of the MYOPIC calculations in a manner identical to those used by the experimenters.

Despite these precautions, agreement with experiment in the high frequency range (>500 Hz) remains less than satisfactory (Figure 4.3) although there has been considerable advance on earlier theoretical efforts.

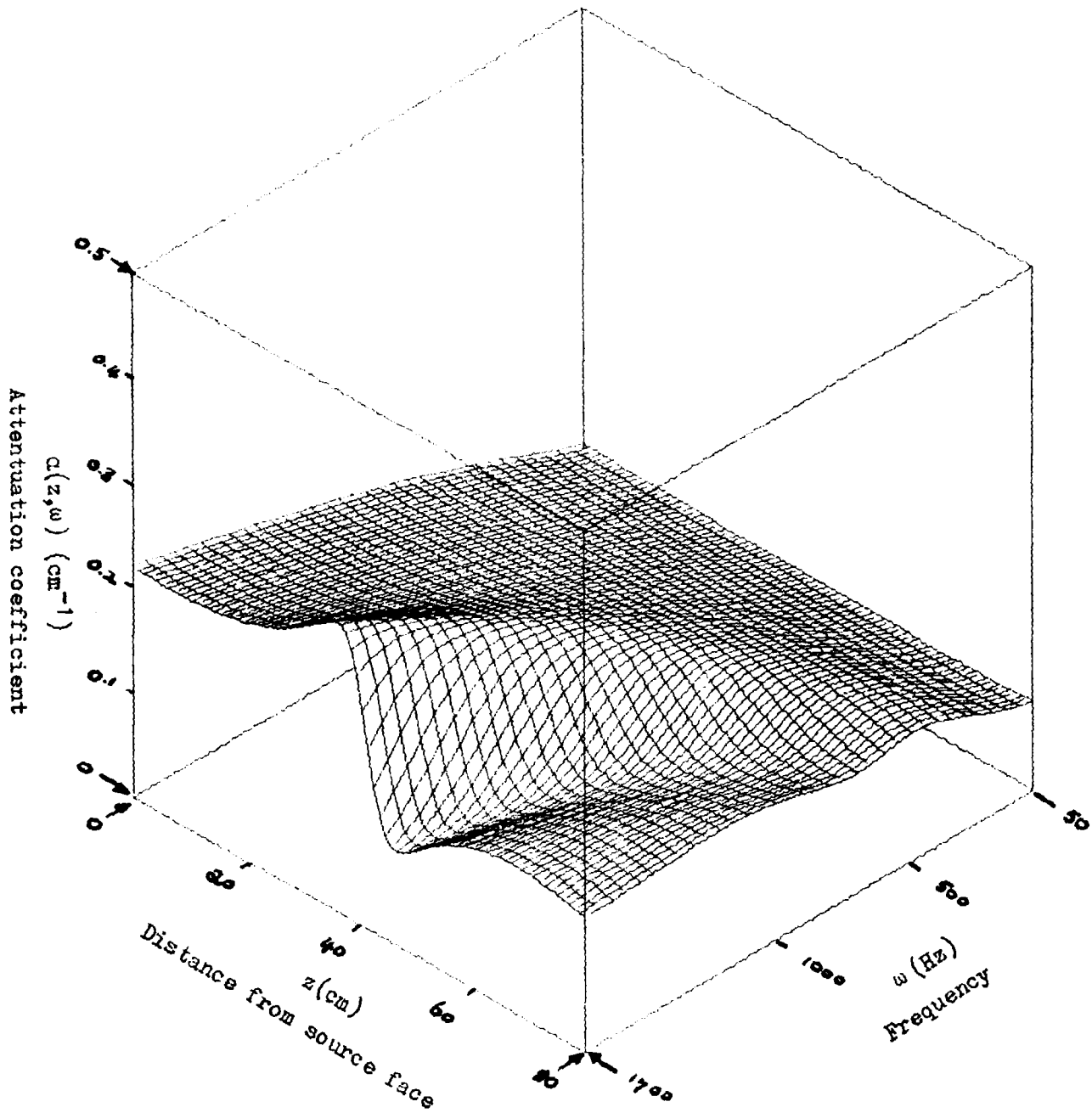

Figure 4.1 Isometric plot of neutron wave attenuation constant $\alpha(z,\omega)$ for beryllium as function of distance and frequency.

300 K Maxwellian source, $B_1^2 = 5.13 \times 10^{-3}$ cm^{-2}

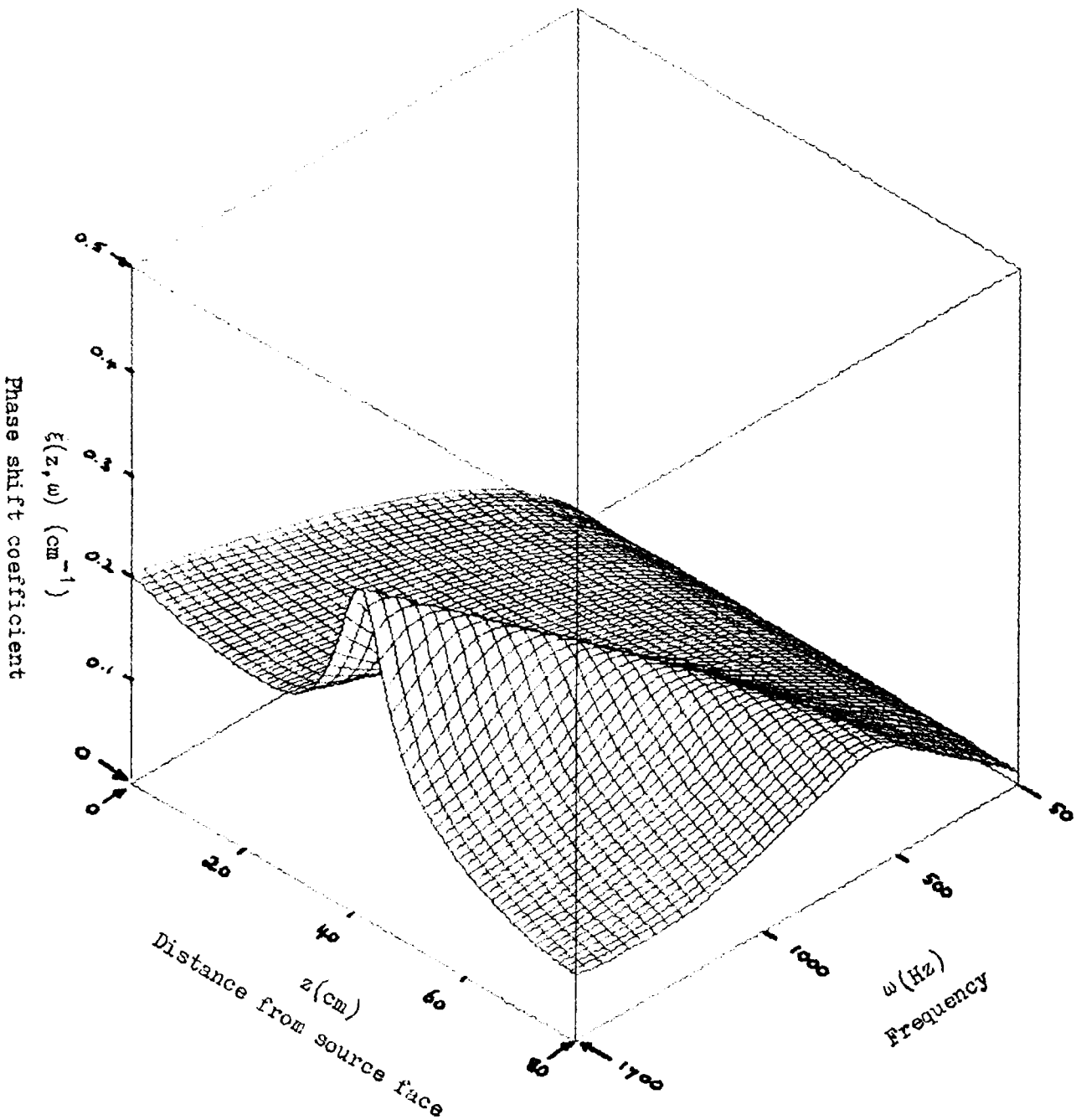

Figure 4.2 Isometric plot of phase shift $\xi(z,\omega)$ of neutron wave as function of distance and frequency.

300 K Maxwellian source, $B_{\perp} = 5.13 \times 10^{-3}$ cm^{-2}

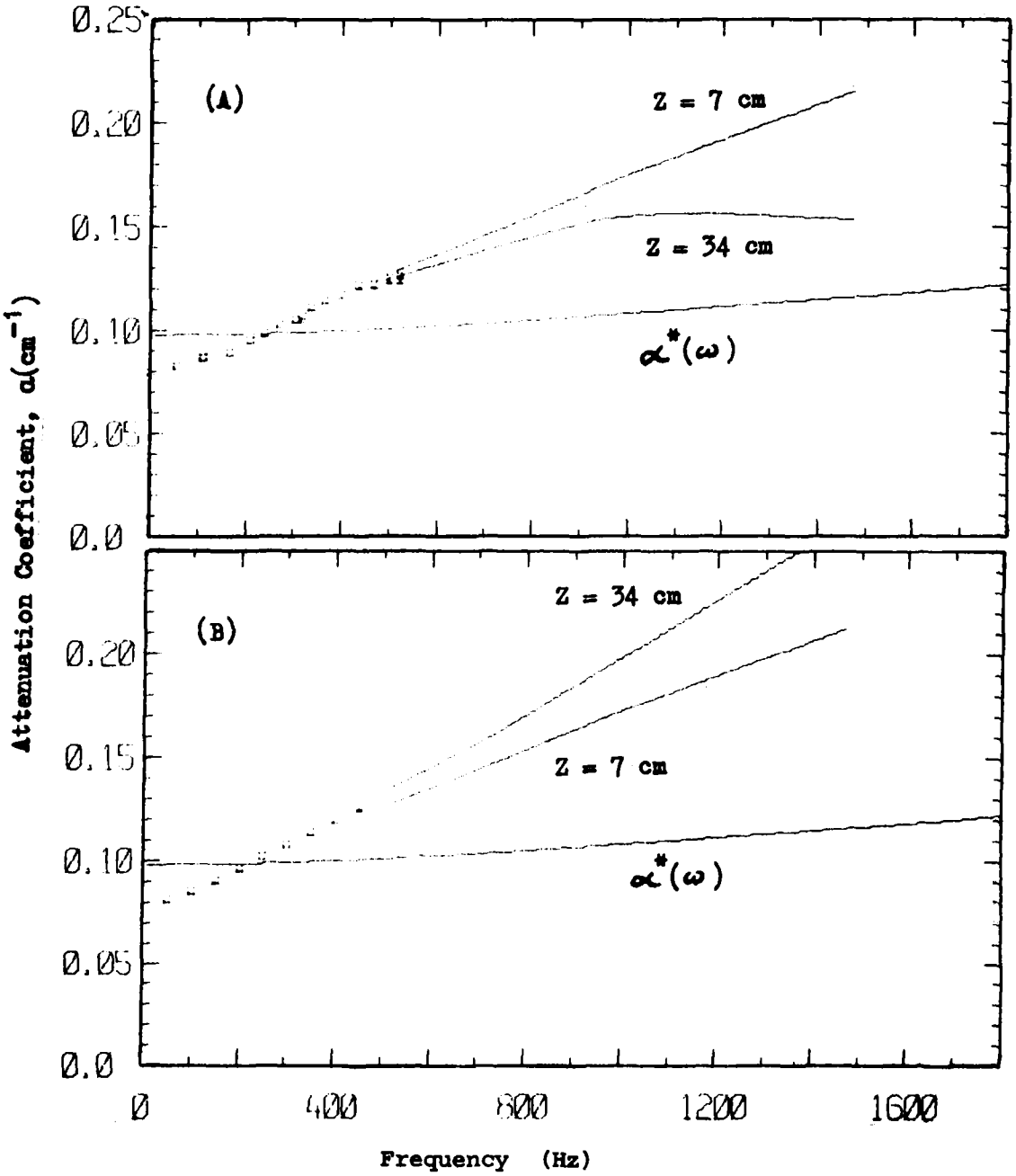

Figure 4.3 Comparison of experimental and calculated BeO attenuation coefficient as function of frequency and distance.
(A) Experiment: Ritchie and Whittlestone (1972, 1973)
(B) MYOPIC calculation

4.6 OTHER ITEMS

Inverse Reaction Problem

For calculation of the behaviour of all fission reactors it is necessary to know or predict the energy dependence of reactor material cross sections in the MeV neutron energy range with some precision. The existing (optical model) theory calculates the total and elastic scattering cross sections with the aid of potential functions - functions of distance from the centre of the interacting system - which represent the processes taking place in the nucleus during nuclear reactions. The inverse reaction problem is to calculate the potential for a system with known cross sections. The standard method of determining a potential is to assume some functional form and to estimate its parameters by comparison of experimental data with that predicted by the potential. For the important case of ^{238}U, various optical model potential functions have been developed in this way to describe its properties at neutron energies of 2, 8 and 14.8 MeV. They are, however, not unique and because they have no known systematic behaviour, cannot be used to predict the potentials at other energies.

There are theoretical grounds for believing that an energy independent potential function should exist and this motivated the present theoretical study of the problem of finding a way to determine such a function directly from experimental data. It is obviously desirable in developing the technique to study a simple nuclear reaction for which a great deal of experimental information is available and the pion-nucleon system was chosen. Reaction matrix theory has been used to develop an energy independent potential for this system and its uniqueness demonstrated under certain conditions. One condition is that only a limited amount of detail in the shape of potential should be extracted from the experimental reaction data, and the technique developed only determines a set of average value of the potential, being that appropriate to a band of distances from the centre of the system. These have been termed 'radially group averaged potentials'.

So far, adequate fits have been achieved for seven important states of the pion-nucleon system. Numerical integration of the Schrödinger equation using our potentials has reproduced the asymptotic phase shifts given by experiment. A new technique has been devised based upon analytic integration of the Schrödinger equation using matching of square well wave functions. Above the inelastic threshold, the method will be applied to the complex phase shifts to calculate the complex optical potentials which reproduce the scattering and reaction data. Using this technique, we are currently repeating

our calculations for the states previously mentioned. When this is completed, we propose to determine the bound states and resonances associated with these states. This calculation is very interesting. The existence of resonances in this system has been well established. Their parameters of width and position have been determined by experimental measurement. As yet, no theoretical examination has succeeded in reproducing these parameters from calculations based on the Schrödinger equation. We hope our calculation will give these parameters.

From the potentials so far computed, a hitherto unsuspected structure has emerged. It appears that with one exception, two wells and two barriers contribute to the shape of the potential. This implies that the excited states of the nucleus, known as nuclear resonances, should fall into two distinct categories of isometric states, without transition between them.

One particular p-state (with angular momentum l=h) contains the nucleus itself as a bound state. With the fitted potentials we have searched for the position of this bound state using real and negative values for the momentum squared of the system. So far we have been unsuccessful. An examination of reaction matrix theory and its predictions for the properties of this state led us to conclude that the bound state may occur at a complex momentum, a situation which can only occur for states with l greater than 0.

The potential evaluation works through a direct search for the group averaged potential which reproduce the asymptotic phase shifts. An error analysis routine is being included to enable us to predict whether a given potential level is significant. One difficulty we found in the past was obtaining a complete set of phase shifts with stated errors on this data. Very recent determinations have provided this data and will permit us to examine the internal structure of the nucleus with a knowledge of the uncertainty on the group averaged potentials calculated.

Interactive Computer System (J. Pollard, G. Trimble)

The Physics Division GT-40 computer system currently comprises a Digital Equipment Corporation PDP-11/10 processer with CRT display screen, to which are connected a card reader and line printer. The system, although it can operate alone, is permanently interfaced to the AAEC Dataway and thus has access to the central IBM 360/50 and other computers on site.

The system has two purposes. The first is to provide batch local input/output of jobs to the central computer. The second is to provide interactive text and graphic facilities, both locally and with the help of the central computer. In such a system, the input/output for the central computer must operate purely in the background. The interactive user should not even be aware that these functions are taking place and the system should appear to this interactive user to be dedicated to his purpose.

In the period under review, most of the software development for the GT-40 system was concerned with making the background tasks function as efficiently as possible. Five specific background tasks have been identified and program segments for these are noramlly resident and operate in the topmost 3K bytes (of a total of 16K bytes) of core storage. These are:

(i) A card reader bootstrap and absolute loader for reading programs into the GT-40.

(ii) A Dataway handler for controlling simultaneous operation on all four available Dataway addresses.

(iii) A Dataway program call routine which allows GT-40 programs to be loaded from the IBM 360.

(iv) A program to accept card decks from the card reader.

(v) A program to accept printed output from the 360 and list it on the local line printer.

Two main programs have been developed for the interactive user. They are:

(i) 'FOCAL-VT' which is based on the Digital Equipment Corporation interpretive language FOCAL. It includes locally written functions to allow the user to construct and modify pictures on the display screen by use of a teletype or light pen.

(ii) 'HASTE' which allows the user to interact with the IBM 360. The user may operate the GT-40 as an 'internal HASP console' and so monitor the progress of his job on the 360. Alternatively,

he may initiate 'link tasks' (small high priority jobs) on the 360 which allow him access to data stored on 360 disks. An example of this latter use is the capacity to preview plot data prepared for drawing by the CALCOMP plotter.

Fossil Fuel Depletion Modelling (K. J. Maher)

The growth of nuclear power is directly related to fossil fuel prices which, in turn, partially reflect the extent to which fossil reserves are depleted. Estimations of the life cycle of reserves are notoriously speculative, but recent serious attempts have been made to construct econometric models of resource usage with the finiteness of the resource a dominant boundary condition.

Naill's (1973)* model of US natural gas depletion, written in the DYNAMO simulation language, has been translated to FORTRAN with the addition of routines that preserve some of the desirable features of DYNAMO and a graphics output capability that is an improvement on DYNAMO.

It is hoped that experience with the translated program, USGAS, will provide initial experience in a new and growing field and that it may lead to the development of an Australian oil and natural gas depletion model.

---

*Naill, R. F. (1973), in 'Towards Global Equilibrium - Collected Papers', Eds. Meadows, D. L. and D. H., Wright Allen Press.

5.1 RUM JUNGLE ENVIRONMENTAL STUDIES (B. E. Clancy and I. Ritchie)

Modelling of the water flow distribution and heavy metal content of water from the Rum Jungle overburden heap should provide a useful tool in assessing measures aimed at mitigating heavy metal pollution from these overburden heaps. Expertise developed during such a study should be applicable to the more general problem of heavy metal leaching from mine waste dumps, in particular those situated in the Northern Territory. However, successful modelling depends crucially on reliable measurements of the phenomena being investigated. The reliability of measurements already done has been assessed and deficiencies in these measurements have led to proposals for new measurements in the coming year.

It has been decided to concentrate mainly on investigating White's overburden heap. This is the largest heap in the area and probably the largest single contributor of heavy metal pollution to the East Finniss River System. It is more homogeneous than Dyson's heap. Its drainage pattern is probably less complex than that of the Intermediate heap.

Spring water flow from White's provided good estimates of water discharge rates during the dry season. The exponential time dependence of the spring water discharge also allowed a good estimate to be made of discharge during the wet season. These estimates indicate that flow from this spring accounts for less than 5 per cent of the rain falling on the heap. Since, from the literature, run-off is not likely to exceed 50 per cent, it would appear that a significant fraction of water goes through to the ground water or appears as very short-lived springs. Attempts to obtain reliable estimates of the run-off fraction on White's heap during the 1974-75 wet season by constructing a weir on the run-off channel were frustrated by cyclone Tracy. Construction work will now take place during the 1975 dry season.

The physical size of the heaps has been rather uncertain, but new data obtained from two independent sources, appears to be internally consistent and indicates considerable departure from previous data. For example, White's heap is 100 per cent larger in area and 30 per cent larger in volume than previous data indicated. The larger physical sizes of the heaps, together with data for spring flow and metal ion concentration in the spring water, has led to revised estimates of the metal burden to the East Finniss river. The total copper burden for all three heaps in a typical year is probably between 30 and 60 tonnes, a major fraction of which comes from White's heap.

However, it should be noted that these figures are based on a number of assumptions on the water flow pattern that may not be valid.

Revised estimates of heap size and metal ion concentration in run-off and spring water led to new estimates of sulphide ore and oxygen consumed in the oxidation process in a typical season. Two different processes could be envisaged:

(i) A volume process involving the heap as a whole, and

(ii) a surface process which, each season, would completely exhaust the sulphide ore in a surface layer. For this process to continue, it would be necessary for the surface layer to be eroded away before the next year's rain.

Several estimates for oxygen and ore consumption indicate that for White's heap the volume process would need an air turnover within the stack of about twenty times a year, compared to previous estimates of about five times, and that the surface layer would have to be between 11 and 19 cm thick compared to previous estimates of about 2 cm. The new data makes the surface layer process much less likely.

The metal ion, SO and total sulphur concentrations were measured in samples taken from trenches dug to a depth of 1.8 m in White's heap. Samples were taken from trenches dug in terrain which included pyrites outcrop, bare and vegetation covered surfaces. Analysis of the results showed that there was no consistent trend with increasing depth either within a trench or within a set of trenches, although individual sets of results could show a variation of a few hundred per cent. Similarly, the variation between samples masked any trend between grass covered and non-grass covered areas. There was, however, a significant decrease of about a factor of four in the average sulphur content of these surface samples, compared to the average for the heap as a whole.

At this stage, it is considered that the oxidation process probably occurs throughout the entire heap and that the main driving mechanism is water flow which causes air movement in the heap and transports out the heavy metal ions. Significant oxidation in the saturated region of the heap (low oxygen solubility in water) is thought unlikely. The more difficult problem of water flow in the unsaturated region therefore has to be studied. Water flow in such a region is described by a time dependent diffusion type equation which can be solved using techniques well known in reactor physics. Preliminary computer experiments have shown that to study detailed flow in a

geometry which approximates that of the heap and covering a time period typical of a rainy season would consume large amounts of computer time.

A method of simplifying the problem and decreasing the computer time required has been devised. The method is closely analogous to the buckling treatment of transverse leakage so familiar in neutron diffusion and, indeed, simplifies the problem by using a buckling term which accounts for the total water leakage out of the sides of the heap. A similar treatment is possible in calculating air flow within the heap. A computer program based on this analysis has been developed and is being tested.

In the coming year it is proposed to carry out water run-off and rainfall measurements on White's heap which will give a more reliable estimate of how the water flow is distributed between run-off, spring and ground water. These measurements, together with measurement of ion concentration, will give more reliable estimates of the oxygen consumed. This quantity can then be compared with predictions by the water and air flow models of the quantity of air transported into the stack. The air turnover rate predicted by the model can also be compared with the generation time of the bacteria, ferrobacilli and thiobacilli, which catalyse the oxidation process.

6.1 PUBLICATIONS

Papers

Bertram, W. K. and Cook, J. L. (1975) - A note on unitarity in resonance theory. Aust. J. Phys. 28, 1.

Boldeman, J. W., Allen, B. J., Musgrove, A. R. deL. and Macklin, R. L. (1975) - Valence component in the neutron capture cross section of ^{90}Zr. Nucl. Phys. A246, 1.

Boldeman, J. W., Allen, B. J., Musgrove, A. R. deL. and Macklin, R. L. (1975) - The neutron capture cross sections of natural silicon - accepted for publication in Nuclear Physics.

Donnelly, I. J. (1975) - A comparions of ANISN and SABINE shielding calculations. NEA Computer Program Library Newsletter No. 18.

Kenny, M. J., Martin, P. W., Carlson, L. E. and Biggerstaff, J. A. (1974) - Gamma ray transitions following keV neutron capture in 2s-1d shell nuclei. Aust. J. Phys. 27, 759.

Musgrove, A. R. deL. (1975) - keV neutron resonance capture in ^{138}Ba - accepted for publication in Nuclear Physics.

Pollard, J. P. (1974) - Floppy rulers and light pens - reactor mathematical aids. J. Proc. Royal Soc. NSW, 107, pp. 116-121.

Walsh, R. L. (1975) - Experimental fission research at Lucas Heights. Atomic Energy in Australia, 18 (2) 2.

Wall, T. and Gillespie, P. (1975) - Neutron radiography at Lucas Heights. Atomic Energy in Australia 18, No. 3, July 1975.

Reports

Bertram, W. K., Clancy, B. E., Cook, J. L. and Rose, E. K. (1974) - The statistical distribution functions for products of variables with a Gaussian distribution with zero mean. AAEC/E313.

Clancy, B. E., Connolly, J. W., Harrington, B.V. (1975) - Analysis of power transients observed in SPERT I power reactors. Part I. AAEC/E345.

Dalton, A. W. (1975) - Review of fuel-coolant interactions and their relevance to the safety of reactors. NSTB/PE4.

Donnelly, I. J. (1975) - The eigenvalues of the discrete ordinate equations in slab geometry. AAEC/E360.

Reports (cont'd)

Harries, J. R. (1974) - The transmutation of radioactive reactor waste. AAEC/E326.

Harries, J. R. (1975) - Correlation and flux tilt measurements of coupled-core reactor assemblies. AAEC/E357.

Harries, J. R. and Wilson, D. J. (1975) - The storage and disposal of high-level radioactive waste - a description of current and proposed methods. NSTB/PE6.

McGregor, B., Harrington, B. (1974) - Comparison of calculations made with three time-dependent neutron codes TDA, MORSE and POW. AAEC/E336.

McGregor, B. (1975) - Comparison of calculations of a reflected reactor with diffusion, S_N and Monte Carlo codes. AAEC/E343.

Musgrove, A. R. deL., Allen, B. J. and Macklin, R. L. (1974) - keV neutron resonance capture in barium-135. AAEC/E327.

Pollard, J. P. (1975) - AUS diffusion module POW checkout - 1 and 2 dimensional kinetics calculations. AAEC/E (in press).

Ritchie, A. I. M. (1975) - Neutron yields and energy spectra from the thick target Li(p,n) source. AAEC/E359.

Robinson, G. S. (1975) - AUS - the Australian modular scheme for reactor neutronics computations. AAEC/E369.

Robinson, G. S. (1975) - AUS burnup module CHAR and the associated STATUS data pool. AAEC/E (in press).

Rose, E. K. and Cook, J. L. (1974) - The statistical distribution functions for product ratios and sums of product ratios. AAEC/E316.

Turner, W. J. and Trimble, G. D. (1975) - Critical review: hydraulics for blowdown analyses of water cooled reactors. NSTB/PE10.

Conference Papers

Allen, B. J., Boldeman, J. W., Kenny, M. J., Musgrove, A. R. deL., Pe, Hla and Macklin, R. L. (1975) - Neutron capture mechanisms in light and closed shell nuclei. Proc. USEAC Conf. on Neutron Cross Sections and Technology, Washington.

Bertram, W. K., Boldeman, J. W., Walsh, R. L. and Caruana, J. (1975) - Calculation of the fission cross section for ^{233}U and the interpretation of fragment anisotropy and fine structure in $\bar{\nu}_p$ and $\bar{E}_K$. 3rd National Soviet Conf. On Neutron Physics, Kiev.

Conference Papers (cont'd)

Bird, J. R. Russell, L. H. and Scott, M. D. (1975) - Review of new methods of prompt nuclear analysis. 3rd Aust. Symp. on Analytical Chem., Melbourne.

Boldeman, J. W., Allen, B. J., Kenny, M. J., Musgrove, A. R. deL. and Macklin, R.L. (1975) - Valence and doorway state effects in neutron capture near closed shells. Proc. 3rd National Soviet Conf. on Neutron Physics, Kiev.

Boldeman, J. W. and Walsh, R. L. (1975) - Fine structure in the neutron emission from ^{252}Cf spontaneous fission fragments. Proc. 3rd National Soviet Conf. on Neutron Physics, Kiev.

Caruana, J., Mathur, J. N., Boldeman, J. W. and Walsh, R. L. (1974) - Angular distribution of fragments from the fission of ^{233}U and ^{235}U. Proc. National Conf. on Nuclear Physics, Trombay, India.

Gillespie, P. and Wall, T. (1975) - Some techniques in neutron radiography. 2nd Aust. Conf. on Sci. and Tech., Adelaide.

Rainbow, M. T. and Ritchie, A. I. M. (1975) - Evaluation of group inelastic cross sections using a pulsed integral method. 3rd National Soviet Conf. on Neutron Physics, Kiev.

Turner, W. J. and Trimble, G. D. (1974) - Critical and near critical two phase flow. 5th Aust. Conf. on Hydraulics and Fluid Mechanics, Christchurch.

Turner, W. J. and Trimble, G. D. (1974) - NAIAD - a different approach to hydraulic calculation. Seminar on Computer Programs for the Analysis of Certain Problems in Thermal Reactor Safety, Ispra.

Turner, W. J. and Trimble, G. D. (1975) - Calculation of two phase compressible flow in a network. 3rd National Computational Physics Conf., University of Glasgow.

Wall, T. and Gillespie, P. (1975) - Some industrial applications of neutron radiography. 9th Filling and Assembly Conf., St. Mary's Filling Factory, NSW.

Walsh, R. L. and Boldeman, J. W. (1974) - Odd-even Z effects in the total energy release in fission. Proc. National Conf. on Nuclear Physics, Trombay, India.

DISTRIBUTION LIST

AAEC/PR41-P

1. Chairman
2. Deputy Chairman
3. Commissioner
4. Head, NS&T Branch
5. Program Manager, Nuclear Science and Applications
6. Program Manager, Power and Energy
7. Program Manager, Uranium Fuel Cycle
8. Site Manager
9. Chief, Materials Division
10. Chief, Physics Division
11. Chief, Engineering Research Division
12. Chief, Chemical Technology Division
13. Chief, Instrumentation and Control Division
14. Chief, Environmental and Public Health Division
15. Chief, Isotope Division
16. Head, Applied Mathematics and Computing Section
17. Head, Mechanical Development Section
18. Head, Regulatory and External Relations Branch
19. Secretary
20. Assistant Secretary
21. Director, Information Services
22. Library
23. Director, Nuclear Plant Safety Unit, Mascot
24. Head, Nuclear Studies Group
25. Mascot Library
26. Professor D. W. George (Chairman, Safety Review Committee)
27. Dr. C. J. Cummins (Safety Review Committee)
28. Mr. D. J. Stevens, Director ARL
29. Controller, Site Information Services
30. Controller, Site Administration
31. Controller, Site Operations
32. Controller, Engineering Services
33. Controller, Site Planning
34. Manager, Commercial Applications
35. Nuclear Materials Officer
36. ASNT
37. Executive Officer, AINSE

38-40 RE Library

41. Washington Office

42-43 London Office

44. Vienna Office
45. Tokyo Office
46. Head, Experimental Reactor Physics Section
47. Head, Neutron Physics Section
48. Head, Theoretical Physics Section
49. Head, Reactor Performance Section
50. Head, Engineering Physics Section
51. Head, Chemical Physics Section
52. Head, Applied Physics Section
53. Head, Health Physics Research Section
54. Head, Radioisotope Services Branch
55. Head, Pharmaceutical & Chemical Products Section

DISTRIBUTION LIST (cont'd)

56. Head, Irradiation Research Section
57. Head, Reactor Operations Section
58-98. W. Gemmell for INDC and Bilateral Agreement correspondents
99. B. Allen
100. J. Boldeman
101. J. Connolly
102. J. Cook
103. P. Duerden
104. G. Durance
105. J. Harries
106. G. Hogg
107. M. Kenny
108. D. Lang
109. B. McGregor
110. A. Musgrove
111. J. Pollard
112. M. Rainbow
113. I. Ritchie
114. J. Tendys
115. W. Turner
116-146. J. R. Bird (for special distribution)
147. D. Byers (University of Canterbury, N.Z.)
148. V. Deniz, (BARC, India)
149. S. Kapoor (BARC, India)
150. N. Veeraraghavan (BARC, India)
151. S. Supadi (BATAN, Bandung)
152. I. Supki (BATAN, Bandung)
153. G. Tyror (AEEW, UK)
154. J. Askew (AEEW, UK)
155-175. Bilateral Agreements (UKAEA 5, US ERDA 11, AECL 5) via H.O.
176-186. Spares